LOW VELOCITY MOVING TARGET DETECTION WITH SYNTHETIC
APERTURE RADAR

A THESIS SUBMITTED TO
THE GRADUATE SCHOOL OF NATURAL AND APPLIED SCIENCES
OF
MIDDLE EAST TECHNICAL UNIVERSITY

BY

GÖRKEM NARİN

IN PARTIAL FULFILLMENT OF THE REQUIREMENTS
FOR
THE DEGREE OF MASTER OF SCIENCE
IN
ELECTRICAL AND ELECTRONICS ENGINEERING

JUNE 2019

Approval of the thesis:

LOW VELOCITY MOVING TARGET DETECTION WITH SYNTHETIC APERTURE RADAR

submitted by **GÖRKEM NARİN** in partial fulfillment of the requirements for the degree of **Master of Science in Electrical and Electronics Engineering Department, Middle East Technical University** by,

Prof. Dr. Halil Kalıpçılar
Dean, Graduate School of **Natural and Applied Sciences** ⎯⎯⎯⎯⎯⎯

Prof. Dr. İlkay Ulusoy
Head of Department, **Electrical and Electronics Engineering** ⎯⎯⎯⎯⎯⎯

Prof. Dr. Seyit Sencer Koç
Supervisor, **Electrical and Electronics Engineering, METU** ⎯⎯⎯⎯⎯⎯

Prof. Dr. Çağatay Candan
Co-supervisor, **Electrical and Electronics Engineering, METU** ⎯⎯⎯⎯⎯⎯

Examining Committee Members:

Prof. Dr. Orhan Arıkan
Electrical and Electronics Engineering, Bilkent University ⎯⎯⎯⎯⎯⎯

Prof. Dr. Seyit Sencer Koç
Electrical and Electronics Engineering, METU ⎯⎯⎯⎯⎯⎯

Prof. Dr. Çağatay Candan
Electrical and Electronics Engineering, METU ⎯⎯⎯⎯⎯⎯

Prof. Dr. Umut Orguner
Electrical and Electronics Engineering, METU ⎯⎯⎯⎯⎯⎯

Assist. Prof. Dr. Gökhan Muzaffer Güvensen
Electrical and Electronics Engineering, METU ⎯⎯⎯⎯⎯⎯

Date: ⎯⎯⎯⎯⎯⎯

I hereby declare that all information in this document has been obtained and presented in accordance with academic rules and ethical conduct. I also declare that, as required by these rules and conduct, I have fully cited and referenced all material and results that are not original to this work.

Name, Last Name: GÖRKEM NARİN

Signature   :

ABSTRACT

LOW VELOCITY MOVING TARGET DETECTION WITH SYNTHETIC APERTURE RADAR

Narin, Görkem

M.S., Department of Electrical and Electronics Engineering

Supervisor   : Prof. Dr. Seyit Sencer Koç

Co-Supervisor   : Prof. Dr. Çağatay Candan

June 2019, 81 pages

Detection of slow moving targets with small radar cross sections (RCS) is a challenging problem for the Ground Moving Target Indication (GMTI) systems. GMTI systems face high false alarm and/or frequent target miss rates for such targets. Synthetic Aperture Radar (SAR) systems, on the other hand, offer sufficiently large target energy return, unfortunately not localized to a point in the SAR image due to target motion. This thesis is focused on the study of two methods for moving target detection in SAR images via processing the unlocalized target signature. The first method uses the effect of the target motion parameters on the target signature. This method aims to focus the unlocalized moving target signature in the SAR image by estimating motion parameters. The results are presented via a point target spotlight SAR imaging simulator developed within the scope of this thesis. Secondly, a novel dynamic programming based approach is presented to detect slow moving targets. Contrary to the former one, this method does not require target motion parameters; instead, it captures the unlocalized signatures in the SAR image by using real-valued reflectivity amplitudes of the image. The performance of the method is illustrated with simulated

and field data containing multiple slow moving targets.

ÖZ

SENTETİK AÇIKLIKLI RADAR İLE DÜŞÜK HIZLI HAREKETLİ HEDEF TESPİTİ

Narin, Görkem

Yüksek Lisans, Elektrik ve Elektronik Mühendisliği Bölümü

Tez Yöneticisi   : Prof. Dr. Seyit Sencer Koç

Ortak Tez Yöneticisi   : Prof. Dr. Çağatay Candan

Haziran 2019 , 81 sayfa

Düşük hıza ve düşük radar kesit alanına (RKA) sahip hareketli yer hedeflerinin tespiti Hareketli Yer Hedefi Tespiti (GMTI) sistemleri için oldukça zorlu bir problemdir. Bu tip hedefler GMTI sistemlerinde yüksek yanlış alarm ve/veya sık hedef kaçırma oranlarına yol açmaktadır. Sentetik Açıklıklı Radar (SAR) sistemleri ile hedeften yüksek enerjiye sahip yansımalar alınabilmekte ancak hedef izi SAR görüntüsü üzerinde hedef hareketine bağlı olarak dağılmış şekilde gözükmektedir. Bu tez kapsamında, hareketli yer hedeflerinin tespiti amacıyla, SAR görüntüsü üzerindeki odaklanmamış hedef izlerinin işlenmesine dayanan iki metot üzerine çalışılmıştır. Birinci metotta hedef hareket parametrelerinin hedef izi üzerindeki etkileri kullanılmakta ve hedef hareket parametrelerinin kestirimi ile dağılmış hedef izi odaklanarak tespit gerçekleştirilmesi amaçlanmaktadır. Bu metoda ilişkin sonuçlar, bu tez çalışması kapsamında geliştirilen nokta hedef SAR benzetim aracı üzerinden sunulmaktadır. İkinci olarak dinamik programlama tabanlı yenilikçi bir metot sunulmaktadır. İlk metodun aksine, bu metot hedef hareket parametrelerinin kestirilmesini gerektirmemektedir. Bunun yerine, hareketli hedefe ilişkin odaklanmamış izler SAR görüntüsündeki piksellerin

vii

yansıtıcılık değerleri kullanılarak tespit edilmektedir. Bu metoda ilişkin sonuçlar birden fazla hareketli hedef içeren benzetim ve saha verisi ile sunulmaktadır.

Anahtar Kelimeler: hareketli hedef tespiti, dinamik programlama, hareketli hedef odaklama, SAR

To my family..

ACKNOWLEDGMENTS

TABLE OF CONTENTS

LIST OF TABLES

TABLES

LIST OF FIGURES

FIGURES

LIST OF ABBREVIATIONS

ATI   Along Track Interferometry

CFAR   Constant False Alarm Rate

CPI   Coherent Processing Interval

DP   Dynamic Programming

DPCA   Displaced Phase Center Antenna

GMTI   Ground Moving Target Indication

GUI   Graphical User Interface

IRF   Impulse Response Function

LFM   Linear Frequency Modulation

LPR   Log Probability Ratio

MC   Monte Carlo

MDV   Minimum Detectable Velocity

MRF   Markov Random Field

PDF   Probability Distribution Function

PRI   Pulse Repetition Interval

RCS   Radar Cross Section

SAR   Synthetic Aperture Radar

SCR   Signal to Clutter Ratio

SINR   Signal to Interference Ratio

SNR   Signal to Noise Ratio

SRTM   Shuttle Radar Topography Mission

STAP   Space Time Adaptive Processing

TBD   Track Before Detect

UWB   Ultra Wideband

CHAPTER 1

INTRODUCTION

1.1 Thesis Motivation and Objective

Detection of slow moving ground targets (such as dismounts) from stand-off distances has become an indispensable need of today's airborne radar systems since the information gathered on these type of targets is crucial to acquire tactical advantage in tactical operations. Synthetic Aperture Radar (SAR) systems have been proven to be valuable systems in airborne surveillance and reconnaissance applications since the developments on digital computing allowed real time processing of collected data at high data rates with sophisticated signal processing algorithms. Providing its own illumination with electromagnetic waves, SAR is capable of imaging at day and night under any weather conditions. SAR systems form a synthetic aperture by the coherent integration of echoes received along the motion of the platform to achieve high resolution ground imaging with small physical antenna. One can draw an analogy between the mentioned SAR principles and uniformly spaced linear array theory. The coherent integration of pulses for a long aperture time suggests that large amount of information on the illuminated scene can be gathered via SAR imaging.

The slow moving ground target's radar echo is generally contaminated by ground clutter, noise and interference signals (jamming or discrete clutter returns from man-made objects). Classical Ground Moving Target Indication (GMTI) systems that provide the detection of fast moving ground targets from airborne platforms usually utilize interference suppression algorithms such as Space Time Adaptive Processing (STAP) which is an adaptive filtering method in both spatial and temporal domains with heavy computational load or Displaced Phase Center Antenna (DPCA) which is a space time

1

processing method to mitigate platform motion induced clutter spread by compensating the platform motion with electronic phase shifting of the receiver aperture. The velocity of the dismount targets however falls below the minimum detectable velocity of GMTI systems as these targets have very low Radar Cross Section (RCS). The rich information content offered by SAR systems tend to fill the gap of GMTI systems on the detection of slow moving targets with low RCS.

The previous work related to slow moving ground target detection with GMTI/SAR systems can roughly be divided into three categories: modified clutter suppression algorithms to enhance the detection performance of GMTI systems, focusing of moving target signatures on SAR images and analysis of micro motion signatures of dismounts. This thesis aims to implement one of the classical approaches which is the focusing of moving target signatures on SAR images. Moving target focusing depends highly on the target motion parameters as it is discussed on the following chapters. The point target focusing results are presented via spotlight SAR target simulator developed within the scope of this thesis. Successful point target focusing results motivated us to apply the same method in the estimation of the moving target motion parameters from a complete SAR image and then utilize these parameters to focus the target.

This thesis also presents a second algorithm which does not require any kind of target motion parameters. The offered algorithm is an illustration of a well-known tracking algorithm, namely Dynamic Programming Track Before Detect (DP-TBD), for the detection of moving targets on SAR images. The successful results of moving target detection without any assumption regarding target motion parameters are presented via real SAR data containing slow moving ground target signatures. The literature does not treat exhaustively of DP-TBD studies in this application to the best of our knowledge.

1.2 Literature Review

Gathering information on ground moving targets (e.g. vehicles, armed or disarmed person) such as location, velocity and moving direction has always been the main

application of radar systems. The choices for the most feasible detection approach for ground moving targets is driven primarily by two target parameters which are the RCS and target velocity. GMTI systems are capable of detecting relatively fast moving ground targets at stand-off distances. Ground moving targets with lower velocities such as tanks and cars have their return echoes oftenly buried under the platform motion induced clutter spectral spread. This enforces the use of novel clutter suppression algorithms. STAP is one of the most sophisticated clutter suppression algorithms and is basically a 2-D filtering method in both spatial and Doppler domains where filter weights are adaptively defined according to clutter power trend in the data. The purpose of STAP is to estimate and suppress the average background interference. Ground moving target such as a walking person on the other hand requires special treatment as this type has both very low speed and very low RCS. At this point SAR based methods can step in to exploit the data on slow moving targets collected for thousands of pulses throughout the high resolution SAR image formation process.

As it was stated previously, STAP is an effective method for GMTI radars to mitigate clutter. However the Doppler return of the slow moving targets would still be insufficient for detection even after classical STAP [1]. The main reason behind this is the estimation of average background interference through STAP becomes inadequate to suppress the discrete clutter components which have generally comparable strength to human target return [2]. Yet there are studies in the literature to enhance the capabilities of classical STAP to detect slow moving targets such as walking person. In [1], the complex slow moving target signature is incorporated into the STAP clutter suppression filter weight calculation to detect only the matching signatures. The moving target motion is characterized as a single rotary motion along with linear velocity induced part. The method is implemented on a two different X band Gotcha data sets [3] . Each pixel of the constructed SAR image of the scene is processed with the modified STAP algorithm. For the case with dismount, there are some promising detection results although there are many poor estimates of the target location among total of 10 time instants. For the case without dismounts, only 1 false alarm appears in 10 time instants. The relatively insufficient performance on the first case is associated with the poor cross range resolution of the Gotcha data set. Generally, in the model based approaches mismatch of the target model and real target motion could result in

a high false alarm and/or miss rate. The cause of the mismatch can be either improperly modelled target signature or strong interference signals that alters the apparent signature of the target as in the case of [1].

SAR may serve as a useful tool for slow moving target detection since the image of the surrounding scene helps to interpret the target behavior when it is combined with classical detection results such as target location, velocity etc. Moving targets on the SAR images are smeared/displaced (in cross range) due to their unknown (and thus uncompensated) velocities [4], [5]. Although the smeared signatures on a properly focused SAR image seems to be a disadvantage for detection, this characteristic can be exploited to identify moving targets. Therefore the vast majority of approaches towards the solution of moving target detection with SAR systems are based on focusing of the smeared moving target signature. In this thesis, slow moving target detection problem on a SAR image is approached by the moving target focusing method in Chapter 3.

In order to turn the smeared/displaced signature of the moving target on the SAR image into an advantage for detection, both [6] and [7] inspect the phase history of the moving target. The range equation constructed for a constant velocity target moving in an arbitrary direction in stripmap image is mathematically manipulated without approximations or assumptions in [6] such that it becomes equivalent to the range equation of a stationary target whose location on the image is determined by the original moving target's location and velocity. The intriguing result is that the equivalent stationary target appears in the stripmap image formed with an equivalent platform velocity which is determined by the original platform velocity and moving target's velocity components . This suggests that once the equivalent platform velocity is known through the estimation of the moving target velocity, the moving target can have a stationary equivalent so that classical SAR image formation techniques (range Doppler, w-k, chirp scaling etc.) can be used. Also the exact equivalence of the range equations implies the perfect range migration correction. Unfortunately, it is stated that this exact equivalence is valid only for non-accelerating targets. An analysis for accelerating targets is presented in Chapter 3 of this thesis by employing Taylor series expansion.

4

The study in [7] also presents an analysis of the phase history of a target moving with constant acceleration in slant range employing a second degree Taylor series expansion of the range equation. It is shown that azimuthal displacement is determined by the slant range velocity component of the moving target, platform velocity and slant range. Main contributors of the azimuthal smearing, on the other hand, are said to be cross range velocity and slant range constant acceleration components of the moving target. Hence the method presented here for the detection of unfocused moving target signatures is sensitive to cross range velocity and slant range acceleration of the moving target. The detection method is applied to a complex SAR image partitioned into patches where each patch is Fourier transformed in azimuth then processed with shear averaging algorithm [8] to estimate phase error. The signal history in the patch is corrected via estimated phase error. After the correction, inverse Fourier transform is applied. The focused patch is then subjected to a sharpness metric such as Muller-Buffington image sharpness metric [9] to indicate the detection of a target. The sharpness metric is said to be proven more reliable than the magnitude of the estimated phase error. The optimal patch size is said to be equivalent to the expected moving target signature and overlapping patches is suggested to enhance the detection performance. It is stated that the computational cost is dominated by 1-D Fourier transforms applied twice during detection algorithm. The proposed method's performance is assessed by simulations and implementation on real data.

In [10], a method based on the work of [7] is given for slow moving target detection on a single channel complex SAR image partitioned into overlapping patches. The detection algorithm includes range migration removal and azimuth phase focusing steps where the former compensates the motion of the moving target in range direction and the latter uses the instantaneous phase difference from pulse to pulse to estimate phase correction sequence. The results are presented on a P band SAR data containing 2 controlled targets walking in cross range. The algorithm is illustrated on both single pass complex SAR image and difference image formed by complex subtraction of multiple pass SAR images. It is observed that difference image eases the detection process by offering increase in signal-to-clutter-ratio (SCR) when it is compared to single pass image.

Focusing the signature of a moving target on the SAR image results in defocusing

of stationary target signatures on the image since the primary assumption of SAR image formation is the stationarity of the illuminated scene. This disrupted background makes it difficult to assess the performance of the focusing method as the signal-to-interference-plus-noise-ratio (SINR) reduces. The difference image formed by multiple pass SAR images is offered in [10] to overcome this adverse effect. The image partitioning offered by [7] increases the SINR for patches containing moving targets. [11] proposes an alternative method which is suitable for both single and multiple pass SAR images. The method operates on a complex SAR image partitioned into sub-apertures (e.g. sub-aperture numbers 2, 3, 5). The purpose is to remove the stationary background on the SAR image such that only smeared/displaced signatures remain prior to focusing algorithm. The background subtraction is basically a non-coherent subtraction of sub-apertures where constant false alarm rate (CFAR) difference statistics is utilized for each sub-aperture. Multiple sub-apertures enables the resulting image to have smooth transitions at the boundaries of sub-apertures. The detection algorithm offered in [11] following background suppression is similar to previously mentioned focusing algorithms in [7] and [10] in the sense that the motion of the moving target is compensated by a set of motion hypotheses. The results of the detection algorithm are presented on a real data with artificially injected moving target signatures. For targets with below minimum detectable velocity (MDV) speeds, results are said to be promising although integration time to form a high resolution SAR image well exceeds the classical GMTI integration time.

Another work on the moving target detection by focusing moving target signatures by hypotheses testing is given in [12]. Similar to abovementioned works, [12] presents analytical expression of moving target range equation followed by the derivation of equivalent platform velocity. The focus of the paper is moving target detection for a ultra wideband (UWB) SAR system. Hence the back projection method is used as a SAR image formation method. The detection results are analyzed on both simulated data and real data with artifically injected moving sea target signatures. It is suggested to use moving target focusing techniques together with multichannel systems in order to benefit from STAP like clutter supression algorithms.

Although focusing of moving target signature is a widely used technique, detection of moving targets from SAR images is not only limited to this method. The micro mo-

tion characteristics of slow moving targets can also be informative. There are several works focusing on modelling micro Doppler and micro range profiles of pedestrians for both airborne and ground based systems [13], [14], [15] and [16].

McDonald and Damini offer amplitude and frequency modulated model for pedestrian motion derived from the observation of X-band wideband airborne radar in [2]. The data is collected for both forward looking and broadside spotlight geometry including controlled targets with typical velocity of 3.5 km/h. The paper refers STAP to enhance the target returns which are buried under clutter due to low target speed.

The study of [17] provides a feature extraction study from a circular SAR data. Range profiles (limb, torso, complete target), Doppler time signatures and range-Doppler data are analyzed in this paper for both low clutter controlled environment with 3.5 cm range resolution and measured real data with range resolution around 20 cm. The examination shows that airborne radar would be insufficient to separate limb and torso scatterers from range profile when it is compared to controlled data in which torso scatterers and limb trajectories are present. The leg micro Doppler returns can be observable in Doppler-time analysis with sufficient clutter suppression in the measured data. The general comment of the paper on the feature extraction of a slow moving target from an airborne radar is that extracting the micro motion information requires sufficiently high SCR.

Lastly, the studies on Track Before Detect methods in the literature regarding moving target detection can be summarized as follows: TBD methods have evolved in order to use the raw target measurement information to the maximum extent to detect and track weak targets. Batch and recursive TBD studies such as particle filter based tracking [18], [19]; Hough transform based sea target tracking [20]; dynamic programming (DP) based maneuvering target tracking [21], [22] can be found in the literature for the detection of low SINR moving targets for infrared and optical sensors. References [21] and [22] employ DP-TBD method to achieve better detection performance on maneuvering targets. Moving target signature appearing in a SAR image is analogous to a slow maneuvering target, since the signature also extends in the cross track direction. Reference [23] studies DP based TBD algorithm for moving target detection on SAR images. The paper applies pre-processing to the SAR

image by partitioning the raw data into sub-images and subtracting the adjacent ones to improve SCR. Pre-processing also includes CFAR threshold. DP-TBD algorithm is then applied to the pre-processed data utilizing the fact that moving target signature in the SAR image shows the same characteristic between adjacent frames. Moving target in a SAR image has a smeared signature with similar pixel intensities forming a line-like signature. Therefore sub-images formed by partitioning the original SAR image have moving target signature pieces showing the similar smear and intensity characteristics. The results show that DP-TBD is a successful candidate to achieve low SCR moving target detection in SAR.

The main interest of this thesis is to investigate the problem of ground moving target detection for airborne platforms with SAR systems which is a branch of SAR/GMTI research field. The related work in the METU EEE Department includes mainly GMTI based solutions which is also useful throughout the development of the work in this thesis. In this thesis, a novel track before detect based approach is also proposed as a solution approach to the mentioned problem. Thesis studies on track before detect topics with motivations other than ground moving target indication can also be found among the METU EEE theses. Related thesis studies can be given as follows:

In [24], space time auto-regressive filtering and model-based GMTI approaches are studied to deal with the heavy computational load and large number of required secondary data problem of the classical clutter suppression algorithms.

In [25], a knowledge based approach is proposed to enhance STAP clutter suppression algorithm. The method makes use of Shuttle Radar Topography Mission (SRTM) data as well as instantaneous platform own ship data as prior knowledge sources.

In [26], a non-adaptive antenna beamforming method which reduces the number of required channels to two is proposed for slow moving target detection to diminish signal processing load.

In [27], several GMTI methods including "Displaced Phase Center Antenna" (DPCA), "Along-Track Interferometry" (ATI), "Adaptive DPCA", "Pre-Doppler Sigma-Delta STAP" and "Post-Doppler Sigma-Delta STAP" are compared through simulation environment.

Among track before detect based research [28] and [29] investigate particle filter based tracking while [30] studies Hough transform based sea target tracking.

1.3 Thesis Outline

Chapter 2 presents the background information regarding SAR data collection and image formation process. Chapter 3 gives the features of moving targets on the SAR image as well as a simulation of moving target focusing algorithm. Chapter 4 discusses the dynamic programming based moving target detection on a SAR image. The implementation of the method is applied to both simulated and real data. Chapter 5 includes comments on the presented material together with the prospective studies on the subject.

CHAPTER 2

BACKGROUND

2.1 SAR Basics

SAR systems produce two dimensional image of the ground scene representing the scatterer distribution on the illuminated scene. In other words, SAR image represents the illuminated scene reflectivity where brighter pixels indicate stronger reflectivity. The two dimensions are called as range (a.k.a.cross track) and cross-range (a.k.a.along track). Although the resolution needed for a comprehensible SAR image is determined by the specific application, sub-meter resolutions in both dimensions are preferred for a detailed SAR image. The range resolution is determined by the signal bandwidth similar to the pulse compression application in the classical radar systems. The wider the bandwidth gets, the finer the range resolution becomes. In a conventional radar with a real beam, the resolution of two scatterers is defined in [31] with the following expression "… *two scatterers are considered just to be resolvable if they are separated by the width of the antenna beam*". The parameters affecting the antenna beamwidth are the antenna aperture dimensions and the operating frequency. The relationship between them is given below:

$$\theta_{az} = \lambda/D, \tag{2.1}$$

where θ_{az} is the antenna beamwidth in the azimuth direction, D is the aperture dimension and λ is the wavelength. Then the cross range resolution, $\Delta xres$, degrades with range (R):

$$\Delta xres \approx R\theta_{az}. \tag{2.2}$$

The dependency of cross range resolution to the range means varying resolution throughout the ground scene. Large aperture or high frequency systems have better

cross range resolution at a fixed range. Unfortunately, cross range resolution needed in SAR systems is often much finer than it can be achieved with real apertures with reasonable dimensions. To illustrate this point let us consider a case of achieving 1 m cross range resolution with an X band system at 10 km range. The real aperture dimension required for such a case would be ~300 m. It is unlikely to have such large dimensions on an aircraft.

The concept of "synthethic aperture" emerged to obtain finer cross range resolution in the 1950s. It states that the coherent integration of the signal returns from a moving platform, which forms the effective aperture as it travels, can achieve finer cross range resolution than the real aperture can offer. Thus a synthetic array is created by means of signal processing. In practical systems, SAR sensor mounted on an airborne platform forms synthetic aperture with the motion of the platform on a straight flight path. The combination of the echoes received from successive positions of the radar implies that the illuminated scene is assumed to be stationary during the data collection For the example given before, 300 m aperture can be formed with an aircraft carrying a small real aperture without any trouble.

Synthetic aperture formation theory is analogous to the linear array theory in the sense that position of the moving platform can be considered as an individual antenna element in a uniformly spaced linear array. In linear array theory, a more directive beam can be achieved via the constructive interference of the individiual fields generated by identical individual antenna elements with a progressive phase. In this case, all the elements transmit or receive at once. Different from the linear array, SAR transmits and receives sequentially as the real aperture travels. The effective aperture and corresponding beamwidth relation for SAR systems is given as:

$$\theta_{SAR} = \lambda/2D_{SAR}, \tag{2.3}$$

where D_{SAR} is the effective aperture length and θ_{SAR} is the corresponding beamwidth. Having 2-way antenna patterns at every sensor position in SAR imaging as oppose to having 1-way patterns of each element in linear array results in an additional 2 factor in the denominator. Synthetic array has half of the beamwidth of a conventional array of the same aperture length.

In the Figure 2.1, a sample SAR image acquired with ASELSAN SARPER$^{\text{TM}}$ SAR

12

Figure 2.1: Sample SAR Image

system is shown. The intensity of an each pixel represents the reflectivity of the scatterers contributing to that pixel in the illuminated area.

SAR systems offers high resolution ground imaging at day and night under any weather conditions. Therefore SAR serves a variety of military applications such as reconnaissance, surveillance, classification, battle damage assessment and locating moving targets on the ground.

2.1.1 SAR Modes

SAR has different modes corresponding to different imaging geometries. The most inclusive ones are called as stripmap and spotlight. Stripmap mode sweeps a long strip of terrain without steering the antenna. A point on the scene can be illuminated as long as the beam sweeps over the point. Hence the cross range resolution is limited with the real antenna beamwidth. Contrary to stripmap, in spotlight mode the antenna beam is steered throughout the flight path to keep the targeted scene illuminated. A point on the scene can be illuminated for a longer time and from different aspects such that cross range resolution enhances with a cost of smaller area coverage. Historically implementation of spotlight follows the stripmap. The finest cross range resolution

can be obtain in stripmap is:

$$D_{az}/2. \tag{2.4}$$

As it can be seen from the equation above, to enhance the cross range resolution azimuth beamwidth should be increased hence physical antenna dimensions should be reduced with the cost of reduced signal to noise ratio (SNR).

To increase the time on target further on a point of interest on the illuminated scene, the scanning of the beam is required so that boresight always points to the point of interest. Spotlight resolution is expressed in terms of the rotation angle of the radar boresight,(γ) is:

$$\lambda/2\gamma. \tag{2.5}$$

The remainder of this chapter will present a general understanding of Spotlight SAR imaging theory as it is closely related to the presented moving target focusing method in this thesis.

2.1.2 Radar Range Equation for SAR

What is called clutter for standard radar systems is the target of interest for SAR systems. If the main purpose is to detect moving ground targets then terrain is again denoted as the clutter similar to the classical radar systems. In line with the context of this thesis, the range equation for SAR system considering terrain as clutter will be presented next.

Standard radar range equation for a point target is given as follows:

$$\text{SNR} = \frac{P_t G_t G_r \lambda^2 \sigma G_{SP}}{(4\pi)^3 R^4 kTBFL}. \tag{2.6}$$

Signal processing gain for a SAR system includes range pulse compression gain $(B\tau)$ and number of pulses coherently integrated for cross range resolution. For T_a aperture time the number of coherently integrated pulses is given as:

$$n_{pulse} = T_a/PRI. \tag{2.7}$$

Aperture time defines the data collection period for SAR.

14

Hence the signal processing gain becomes:

$$G_{SP} = \frac{B\tau T_a}{PRI}.$$ (2.8)

Then radar range equation for SAR is given as:

$$\text{SNR}_{SAR} = \frac{P_t G_t G_r \lambda^2 \sigma \tau T_a}{(4\pi)^3 R^4 kTFLPRI}.$$ (2.9)

Aperture time for a Spotlight SAR can be given as:

$$D_{SAR} = v_p T_a,$$ (2.10)

$$\theta_{SAR} = \frac{\lambda}{2v_p T_a},$$ (2.11)

$$\Delta x = \frac{\lambda R}{2v_p T_a},$$ (2.12)

$$T_a = \frac{\lambda R}{2v_p \Delta x}.$$ (2.13)

Note that aperture time is proportional to range which means that resolution is constant with respect to range.

The range equation of SAR then becomes:

$$\text{SNR}_{SAR} = \frac{P_t G_t G_r \lambda^3 \sigma \tau}{(4\pi)^3 R^3 kTFLPRI2v_p \Delta x}.$$ (2.14)

SNR for a point target in SAR increases with finer cross range resolution [31].

Ground clutter RCS can be modelled as an area scatterer:

$$\sigma_{clutter} = \sigma_0 \Delta x \Delta y.$$ (2.15)

Substituting clutter RCS into equation 2.14, Clutter to Noise Ratio (CNR) becomes:

$$\text{CNR}_{SAR} = \frac{P_t G_t G_r \lambda^3 \sigma_0 \Delta y \tau}{(4\pi)^3 R^3 kTFLPRI2v_p}.$$ (2.16)

CNR decreases with finer range resolution [31].

The explanations of the symbols are given in Table 2.1

Table 2.1: Radar Range Equation Symbology

Symbol	Explanation
P_t	Transmitted Peak Power
G_t	Transmit Antenna Gain
G_r	Receive Antenna Gain
λ	Wavelength
σ	Target RCS
G_{SP}	Signal Processing Gain
R	Range to Target
k	Boltzmann's Constant
T	Standart Temperature
B	Bandwidth
F	Noise Figure
L	System Losses

2.2 SAR Data Collection

SAR data collection geometry for spotlight SAR mode is given in Figure 2.2. Range to a stationary target located at $(x_0, y_0, 0)$ is given as:

$$R_0(t) = \sqrt{(x_0 - x_{pi})^2 + (y_0 - v_p t - y_{pi})^2 + z_{pi}^2},$$

(2.17)

where v_p is the platform velocity in the y direction. (x_{pi}, y_{pi}, z_{pi}) is the initial platform location. Transmitted signal model is given below:

$$x_t(t) = p(t)e^{j2\pi f_c t}.$$

(2.18)

The exponential term denotes complex carrier signal model and $p(t)$ includes waveform model (single pulse, LFM, phase coded etc.). The received echo is the time shifted and scaled version of the transmitted pulse with a time shift proportional to target range. The received echo signal model is given as:

$$x_r(t) = \alpha x_t(t - 2R_0(t)/c) = \alpha p(t - 2R_0(t)/c)e^{j2\pi f_c(t - 2R_0(t)/c)}$$
$$= \alpha p(t - 2R_0(t)/c)e^{j2\pi f_c t}e^{-j4\pi R_0(t)/\lambda}.$$
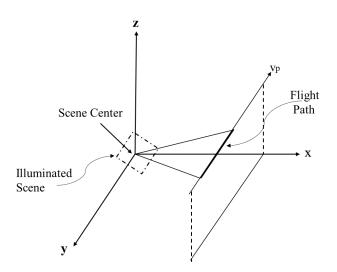
(2.19)

16

Figure 2.2: Spotlight SAR Imaging Geometry

The PRF values for SAR systems is chosen to allow unambiguous operation range not to have overlapping echoes from two different ranges.

2.3 SAR Image Formation

Polar Format Algorithm (PFA) is one of the most widely used spotlight SAR image formation algorithms. The data collected from the illuminated terrain in spotlight SAR mode essentially samples the Fourier transform of the terrain reflectivity hence it requires 2-D inverse Fourier Transform to uncover the terrain reflectivity. The computationally efficient way of 2-D Fourier Transform would be Fast Fourier Transform which needs uniformly spaced samples [32]. PFA emerges as a 2-D polar to rectangular interpolation method that enables to employ 2-D FFT techniques on samples collected in polar format. To reduce computational cost introduced by the interpolation filter, the 2-D interpolation can be realized with successive 1-D interpolation filter implementation in range and cross range dimensions [32].

In the scope of this thesis, separable Keystone interpolation method is performed as described in [32]. The polar samples shown in Figure 2.3 with black dots. Range interpolation of polar samples to horizontal lines is followed by interpolation of range interpolated samples to vertical lines called as cross range interpolation. Cross range
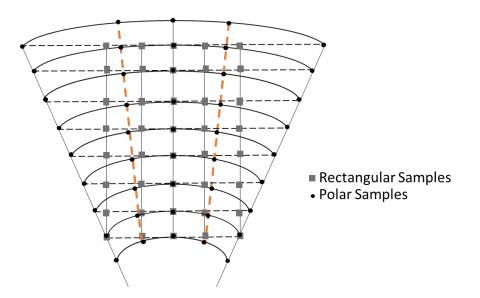
17

Figure 2.3: Polar to Rectangular Sampling Illustration

interpolation data are unevenly spaced contrary to uniformly spaced range interpolation data such that sample separation increases towards the edge [32].

CHAPTER 3

SLOW MOVING TARGET DETECTION ON SAR IMAGES BY FOCUSING

SAR imaging relies on the stationarity of the illuminated scene. Moving scatterers in the scene appear as defocused (smeared) and/or displaced on SAR images due to their unknown thus uncompensated motion components. Analyzing SAR response of a moving point scatterer provides an opportunity to employ these target motion specific features in the moving target detection process. The SAR response of each scatterer is determined by the scatterer's phase history which depends on the distance between the scatterer and the SAR aperture. It can be shown that under certain conditions the distance between a moving scatterer and SAR aperture is equivalent to the one that is between a stationary scatterer and SAR aperture at all time instants during data collection period. In other words, a moving scatterer may appear as a focused stationary scatterer on the SAR image under certain conditions. Therefore, focusing a moving target can be possible once these conditions are met. The next sections describe SAR phase history construction for both moving and stationary targets and present a moving target focusing method which is based on the equivalence of the phase histories [33], [34], [31], [6]. At the end, the performance of the presented method is illustrated on a simulation environment.

3.1 Moving Point Target Phase History

To analyze the focused signature of a single point scatterer, i.e., Impulse Response Function (IRF), first phase history of a point scatterer needs to be constructed. Phase history is stored in the transmitted waveform independent term in equation 2.19 which

is given as $\exp(-j\psi(t))$ where

$$\psi(t) = \frac{4\pi R_t(t)}{\lambda}. \tag{3.1}$$

$R_t(t)$ represents the relative target range with respect to the SAR aperture.

Examination of equation 3.1 shows that two scatterers in the scene which have exactly the same relative range values at all time instants during the data collection period would have the same response. Since Doppler shift is determined by the range rate, Doppler frequency shifts would be equal too [35].

Data collection geometry given in Figure 2.2 is used in the following analysis to define both moving and stationary point scatterers in the scene.

The range to a single point target moving in an arbitrary direction on the scene is given as:

$$R_{tm}(t) = \sqrt{(x_i + v_{tx}t - x_{pi})^2 + (y_i + v_{ty}t - v_p t - y_{pi})^2 + (z_i - z_{pi})^2}, \tag{3.2}$$

where x_i, y_i and z_i indicate initial target position according to Figure 2.2. Target is on the ground hence z_i is zero. v_{tx} and v_{ty} denote target velocity components in the cross track and along track directions respectively. v_p shows the platform velocity and x_{pi}, y_{pi} and z_{pi} define the initial position of the platform.

Using $R_{tm}^2(t)$ and arranging terms with respect to descending powers of t yields:

$$R_{tm}^2(t) = [v_{tx}^2 + (v_{ty} - v_p)^2]t^2 + 2[(x_i - x_{pi})v_{tx} + (y_i - y_{pi})(v_{ty} - v_p)]t$$
$$+ (x_i - x_{pi})^2 + (y_i - y_{pi})^2 + (z_i - z_{pi})^2. \tag{3.3}$$

Range to a stationary point target located at $(x_0, y_0, 0)$ is then:

$$R_{ts}(t) = \sqrt{(x_0 - x_{pi})^2 + (y_0 - v_p t - y_{pi})^2 + z_{pi}^2}. \tag{3.4}$$

Similar arrangement of the terms in the square of the range for the stationary point target yields:

$$R_{ts}^2(t) = v_p^2 t^2 - 2(y_0 - y_{pi})v_p t + (x_0 - x_{pi})^2 + (y_0 - y_{pi})^2 + z_{pi}^2. \tag{3.5}$$

Moving and stationary point targets produce identical responses in a SAR image when $R_{ts}(t) = R_{tm}(t)$ or $R_{ts}^2(t) = R_{tm}^2(t)$ for all time index t during the data collection

period. Received signal is formed by "stop and hop" assumption since the pulse duration is much shorter than the time elapsed between successive antenna positions. Therefore, for N number of pulses, time index (t) can be defined within the range of $[\frac{-NPRI}{2}, \frac{NPRI}{2}]$ with steps of PRI. Equating the coefficients of the second order term defines a circle with the radius v_p, centered at $(v_p, 0)$, i.e.:

$$v_p^2 = [(v_{ty} - v_p)^2 + v_{tx}^2]. \qquad (3.6)$$

v_{tx} and v_{ty} must be on this circle to satisfy equation 3.6 [35]. This means that any moving scatterer with velocity components satisfying the equation 3.6 can be mapped to a stationary target whose location is derived from $R_{ts}(t) = R_{tm}(t)$ equivalence of lower order terms. In other words, any target velocity outside this circle results in defocused signature which is the general case.

A different interpretation of equation 3.6 would be considering an equivalent platform velocity, i.e. v_{pe}, for the stationary target imaging geometry via moving target imaging parameters [6]:

$$v_{pe} = \sqrt{(v_{ty} - v_p)^2 + v_{tx}^2}. \qquad (3.7)$$

In other words, a moving point target initially located at x_i, y_i and $z_i = 0$ position on the scene which is illuminated by a radar with v_p platform velocity has exactly the same range equation as a stationary point target illuminated by a platform with v_{pe} velocity. Location of the stationary target is again determined by the equivalence of the lower order terms in $R_{ts}(t) = R_{tm}(t)$ equation. The corresponding stationary target location can be expressed in terms of the moving target imaging parameters of $x_i, y_i, v_p, v_{pe}, v_{tx}$ and v_{ty}:

$$y_0 = y_{pi} - \left(\frac{(x_i - x_{pi})v_{tx} + (y_i - y_{pi})(v_{ty} - v_p)}{v_{pe}} \right), \qquad (3.8)$$

$$(x_0 - x_{pi})^2 = \frac{[(x_i - x_{pi})(v_{ty} - v_p) - v_{tx}(y_i - y_{pi})]^2}{v_{pe}^2}, \qquad (3.9)$$

$$x_0 = x_{pi} \pm \left(\frac{(x_i - x_{pi})(v_{ty} - v_p) - v_{tx}(y_i - y_{pi})}{v_{pe}} \right). \qquad (3.10)$$

Thus the moving target range equation can be expressed as:

$$R_{tm}(t) = \sqrt{((y_0 - y_{pi}) - v_{pe}t)^2 + (x_0 - x_{pi})^2 + z_{pi}^2}. \qquad (3.11)$$

21

This means that a moving scatterer located at x_i, y_i initial position with v_{tx}, v_{ty} velocity components illuminated by a radar on a platform with v_p velocity has an equivalent range history to that of a stationary scatterer's located at x_0, y_0 initial position illuminated by a radar on a platform with v_{pe} velocity. When the moving target performs only cross track movement, i.e., $v_{ty} = 0$, the equivalent platform velocity and corresponding location of the moving target are given as:

$$v_{pe} = \sqrt{v_{tx}^2 + v_p^2}, \tag{3.12}$$

$$y_0 = y_{pi} - \left(\frac{(x_i - x_{pi})v_{tx} - (y_i - y_{pi})v_p}{v_{pe}} \right), \tag{3.13}$$

$$x_0 = x_{pi} \pm \left(\frac{-v_{tx}(y_i - y_{pi}) - (x_i - x_{pi})v_p}{v_{pe}} \right). \tag{3.14}$$

The cross track velocity component of the target results in a displacement of the moving target's initial position on the focused image. When the moving target performs only along track movement, i.e., $v_{tx} = 0$, the equivalent platform velocity and corresponding location of moving target are given as:

$$v_{pe} = \pm(v_{ty} - v_p), \tag{3.15}$$

$$x_0 = x_i, \tag{3.16}$$

$$y_0 = y_i. \tag{3.17}$$

A moving target with only along track velocity appears at its initial location on the SAR image experiencing no displacement after focusing.

The exact equivalence of a moving scatterer to a stationary one in terms of phase response is demonstrated above for the special case of constant velocity motion of the scatterer. If the motion of the scatterer is not a linear one (due to velocity change, direction change, micro Doppler...etc), this equivalence is no longer exact [6].

To analyze the effects of the higher order components, let us define the target range for an accelerating moving target as:

$$R_{tm}(t) = \sqrt{(x_i + v_{tx}t + \frac{1}{2}a_{tx}t^2 - x_{pi})^2 + (y_i + v_{ty}t + \frac{1}{2}a_{ty}t^2 - v_pt - y_{pi})^2 + z_{pi}^2}. \tag{3.18}$$

Taylor approximation about t yields:

$$R_{tm}(t) \approx R_0 + t\left(\frac{1}{R_0}[v_{tx}(x_i - x_{pi}) + (y_i - y_{pi})(v_{ty} - v_p)]\right)$$
$$+ \frac{t^2}{2}\left(-\frac{1}{R_0^3}[v_{tx}(x_i - x_{pi}) + (y_i - y_{pi})(v_{ty} - v_p)]^2\right. \tag{3.19}$$
$$\left.+ \frac{1}{R_0}[a_{tx}(x_i - x_{pi}) + v_{tx}^2 + (v_{ty} - v_p)^2 + a_{ty}(y_i - y_{pi})]\right),$$

where

$$R_0 = \sqrt{(x_i - x_{pi})^2 + (y_i - y_{pi})^2 + z_{pi}^2}. \tag{3.20}$$

The instantaneous Doppler frequency variation, f_a, is given as follows:

$$f_a(t) = \frac{1}{2\pi}\frac{d\psi(t)}{dt} = \frac{2}{\lambda}\frac{dR_{tm}(t)}{dt} = f_{DC} + k_a t + q t^2, \tag{3.21}$$

When,

$$k_a = \frac{2}{\lambda R_0}[a_{tx}(x_i - x_{pi}) + v_{tx}^2 + (v_{ty} - v_p)^2 + a_{ty}(y_i - y_{pi})$$
$$- \frac{1}{R_0^2}(v_{tx}(x_i - x_{pi}) + (y_i - y_{pi})(v_{ty} - v_p))^2] \tag{3.22}$$

and

$$f_{DC} = \frac{2}{\lambda R_0}[v_{tx}(x_i - x_{pi}) + (y_i - y_{pi})(v_{ty} - v_p)]. \tag{3.23}$$

The second order term of $f_a(\cdot)$ is not of interest in the context of this analysis. Observing the Doppler frequency variation of a moving scatterer enables to associate the scatterer's motion components with the smearing and displacement features on the SAR image. For a stationary target located at x_0, y_0 location, the Doppler history is given as:

$$f_{a,st}(t) = f_{DC,st} + k_{a,st}t, \tag{3.24}$$

$$k_{a,st} = \frac{2}{\lambda R_{0,st}}\left(v_p^2[1 - \frac{1}{R_{0,st}^2}(y_0 - y_{pi})^2]\right), \tag{3.25}$$

$$f_{DC,st} = -\frac{2}{\lambda R_{0,st}}[(y_0 - y_{pi})v_p], \tag{3.26}$$

where

$$R_{0,st} = \sqrt{(x_0 - x_{pi})^2 + (y_0 - y_{pi})^2 + z_{pi}^2}. \tag{3.27}$$

For a stationary scatterer with $(y_0 - y_{pi}) = 0$, $f_{a,st}(t)$ becomes equal to $k_{a,st}t$. This suggests that frequency variation of a stationary target shows resemblence to an LFM signal with a chirp rate of $\frac{2}{\lambda R_{0,st}}v_p^2$ [36].

$R_{tm}(t)$ can be expressed in terms of k_a and f_{DC} as follows:

$$R_{tm}(t) = R_0 + \frac{\lambda}{2}f_{DC}t + \frac{\lambda}{4}k_a t^2. \tag{3.28}$$

Next sections describe displacement and smearing features experienced by moving targets and present the relation of these features to Doppler and range histories.

3.2 Effects of Target Motion on SAR Image

Phase history of a scatterer is a valuable information to analyze the effects of scatterer's motion parameters on its SAR signature features. For a moving target, the effects of target motion parameters on target range history can also be associated with the displaced and/or smeared target signature on the SAR image since phase history is determined by the target range variation. The research studies on the moving target SAR features stem from the early work of Raney [37]. Raney states that along track motion of the target results in smearing of the target signature in the along track direction as well as decreased peak amplitude of the IRF since the signal energy also smears throughout multiple cells. Across track motion on the other hand leads to displaced target signature on the SAR image. These effects can be analyzed via examination of target's Doppler frequency history and range history. The change in the range curvature describing the relative target position with respect to the platform indicates a quadratic phase error whose corresponding effect on the SAR image would be the smearing of the target signature. Similarly, change in the Doppler slope results in a smeared signature. Displacement of the target signature on the SAR image shifts Doppler history and range curves.

3.2.1 Displacement Effects

The main assumption lying behind the SAR image formation algorithms is that all scatterers in the illuminated scene are stationary. Hence, range cell migration of sta-

24

tionary scatterers due to the platform motion is corrected based on this assumption. Stationary scatterers, then, appear on the focused SAR image where their Doppler frequency shifts are zero after the range cell migration correction [36]. These positions correspond to their actual positions on the scene while for moving targets the positions where their Doppler shifts are zero, do not represent their true locations due to their unknown Doppler frequency shift contributors. This displaced signature is known as the 'Train Off the Track Effect' for moving targets.

Moving target's Doppler frequency shift due to its own velocity translates into the displacement of the target signature in along track direction on the SAR image. SAR image is formed only after all the echoes are collected along the synthetic aperture. Therefore, appeared location of moving target on the final image, whether displaced or not, reflects the real location of the target at some point during data collection interval. For a displaced moving scatterer, generally this point is considered as the location at the mid point of the data collection interval [34], [31], [6].

The Doppler frequency of a moving target on the scene is given as:

$$f_{Dm} = \frac{2v_p \cos(\theta) \cos(\phi)}{\lambda} + \frac{2v_t \cos(\theta + \theta_t) \cos(\phi)}{\lambda}, \tag{3.29}$$

where θ is the angle between target's initial position and platform velocity vector. θ_t is the angle of target velocity vector with respect to y axis. ϕ is the elevation angle of the platform. Platform velocity is in the y direction. Imaging geometry is shown in Figure 3.1.

The second term represents the frequency shift resulted from the radial velocity component of the target. If one expresses the equivalent Doppler frequency of a stationary target as:

$$f_{Ds} = \frac{2v_p \cos(\theta_e) \cos(\phi)}{\lambda}. \tag{3.30}$$

Then θ_e can be defined to have $f_{Dm} = f_{Ds}$:

$$\theta_e = a \cos \left(\cos(\theta) + \frac{v_t}{v_p} \cos(\theta + \theta_t) \right). \tag{3.31}$$

The along track location of the stationary target is given as:

$$y_e = R_t \cos(\theta_e) \cos(\phi), \tag{3.32}$$
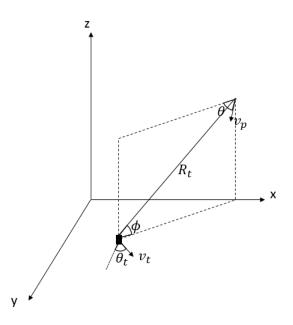
where R_t is the target range.

25

Figure 3.1: SAR Imaging Geometry for a Moving Target

Substituting equation 3.31 into equation 3.32 results in:

$$y_e = R_t \cos(\theta) \cos(\phi) + R_t \frac{v_t}{v_p} \cos(\theta + \theta_t) \cos(\phi). \tag{3.33}$$

The equivalent along track location of a moving target can be expressed in terms of target's initial position (x_i, y_i) and velocity components:

$$y_e = y_i + R_t \cos(\phi) \left(\frac{v_t \cos(\theta_t) \cos(\theta) - v_t \sin(\theta_t) \sin(\theta)}{v_p} \right), \tag{3.34}$$

$$y_e = y_i + R_t \cos(\phi) \left(\frac{v_{ty} \cos(\theta) - v_{tx} \sin(\theta)}{v_p} \right). \tag{3.35}$$

The along track displacement of the moving target from its initial position can be expressed in terms of slant range:

$$\delta_y = R_t \frac{v_t}{v_p} cos(\theta + \theta_t) cos(\phi), \tag{3.36}$$

$$\delta_y = -R_t \frac{v_r}{v_p}, \tag{3.37}$$

where v_r is the radial velocity of the target. This displacement expresses the ambiguity in along track location of the target with cross track velocity [11]. It takes place to either left or right to the real target location by the same amount according to target's

26

heading with respect to the platform. If the target approaches the platform in radial direction, then its signature shifts in the platform heading direction and vice versa.

Figures 3.2 and 3.3 show the range and Doppler history variations of a moving target in the cross track direction with respect to a stationary one respectively. The displacement experienced by such a target is shown as shifts of the range and Doppler history curves respectively.
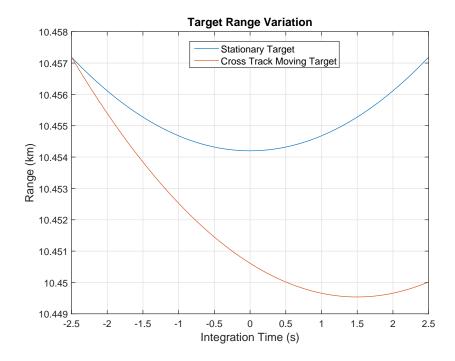
Target Range Variation

Figure 3.2: Range Variation for Cross Track Moving Target

3.2.2 Smearing Effects

Smearing of the target signature in the along track direction on the SAR image is the other effect experienced by a moving target due to its motion components. There is no direct derivation of the smeared IRF in the literature to the best of the writer's knowledege. Although, [36] describes the length of the smear by employing the mismatch between moving and stationary target Doppler slopes. SAR imaging algorithms utilize a matched filter bank to excite each stationary scatterer depending on the minimum phase difference. Exposing moving targets to these filters results in mismatch
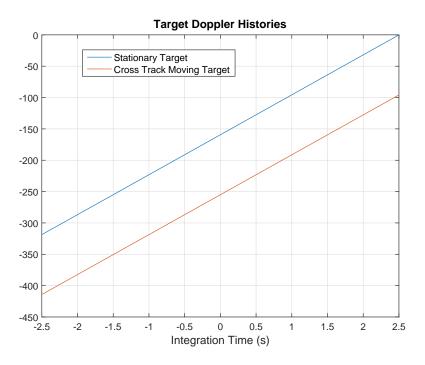
Figure 3.3: Doppler History of Cross Track Moving Target

due to their distorted phase terms. This mismatch is the reason for displacement and smearing of the moving target signatures and can be expressed in terms of the target Doppler history. Doppler slope of a moving target is represented by the parameter k_a as expressed in equation 3.21. The approximate along track smearing extent can be expressed in terms of the k_a and $k_{a,st}$ mismatch where $k_{a,st}$ is the Doppler slope of a stationary target:

$$\Delta_{az,blur} = \left| 1 - \frac{k_a}{k_{a,st}} \right| T_{ill} v_p, \tag{3.38}$$

where T_{ill} is the illumination time and the term in absolute value is given as:

$$\left| 1 - \frac{v_{tx}^2 + (x_i - x_{pi})a_{tx} + (v_{ty} - v_p)^2 + (y_i - y_{pi})a_{ty} - \frac{[(x_i-x_{pi})v_{tx}+(y_i-y_{pi})(v_{ty}-v_p)]^2}{R_0^2}}{v_p^2 - \frac{(y_i-y_{pi})v_p^2}{R_0^2}} \right| \tag{3.39}$$

As it can be seen from equation 3.39 the main contributors of the along track smearing are the along track velocity, across track acceleration, along track acceleration and across track velocity of the target. The last two have minor effects on the smearing when they are compared to other contributors. On the other hand, very small changes in the across track velocity result in considerable amount of smearing in the along

28

track direction.

Long integration times may result in target smearing to an extent that the decreased peak amplitude of IRF results in miss during target detection phase due to very low SCR. Both along track velocity and the across track acceleration have a contribution to the target smearing which cannot be examined separately according to equation 3.39.

Figures 3.4 and 3.5 show the range and Doppler history variations of a moving target in along track direction with respect to a stationary one. The smearing experienced by such a target is shown as the slope change of the range and Doppler history curves respectively.
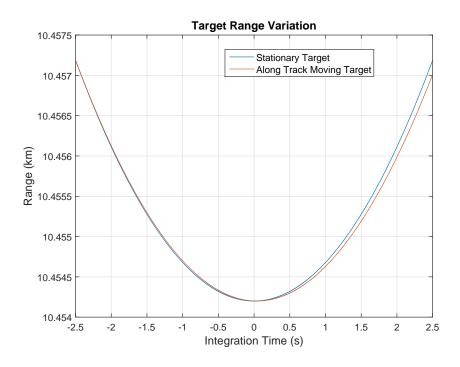

Figure 3.4: Range Variations for Along Track Moving Target

3.2.3 Residual Range Migration

The uncompensated range migration of a moving target is known as residual range migration. This leads to target signature smearing in across track direction. Un-
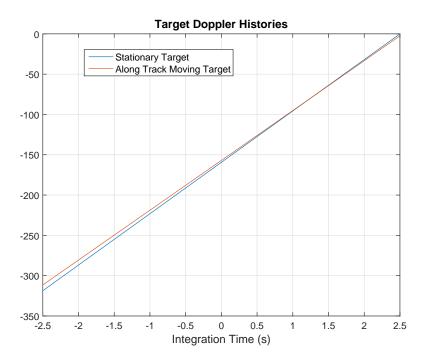
Figure 3.5: Doppler History of Along Track Moving Target

compensated range migration of a moving target can be expressed in terms of the difference between range histories of moving and stationary scatterers. Range history of a moving scatterer as a function of Doppler frequency is obtained by expressing equation 3.28 in terms of $t = \frac{f_a - f_{DC}}{k_a}$:

$$R_{tm}(f_a) = R_0 - \frac{\lambda}{4} \frac{f_{DC}^2}{k_a} + \frac{\lambda}{4} \frac{f_a^2}{k_a}. \tag{3.40}$$

Similarly for a stationary target, range history in terms of Doppler frequency is:

$$R_{ts}(f_{a,st}) = R_{0,st} - \frac{\lambda}{4} \frac{f_{DC,st}^2}{k_{a,st}} + \frac{\lambda}{4} \frac{f_{a,st}^2}{k_{a,st}}. \tag{3.41}$$

Residual range migration is then given as [36]:

$$\Delta_r = R_{tm}(f_a) - R_{ts}(f_{a,st}). \tag{3.42}$$

One moving target motion component that is not discussed yet is the along track acceleration. The main effect of along track acceleration component is a deflection in Doppler frequency curve due to third order phase errors. Consequently IRF of the moving target has unbalanced sidelobes [36].

3.3 Moving Target Focusing

3.3.1 Method

In this work, all the stationary scatterers in the scene are assumed to have ideal responses so that any distortion is caused by the unknown motion of the target. Employing displacement of moving target in detection process makes detection approach sensitive to cross track velocity component of the target whereas using the smearing of the target makes detection process sensitive to along track velocity component of the target and acceleration in cross track velocity. As long as the correct target parameters are known (either estimated or known beforehand), it is possible to generate a matched filter that focuses the smeared moving target signature. However, in practice target related parameters are unknown. If this is the case, one method to focus a moving target signature is the application of a matched filter bank with different parameter sets. The one that maximizes the SCR (peak amplitude of IRF) also provides an estimate of the target parameter set. As suggested in [36], the matched filter bank can be seen as the maximum likelihood estimate of motion parameters. Focusing a smeared signature has no effect on the displacement of the signature, if there is any.

3.3.2 Simulation Results

In this section, a point target IRF simulator is described together with the moving target focusing illustrations.

3.3.2.1 Point Target Simulator Data Generation

Point target simulator implements polar format SAR image formation algorithm to obtain the IRF. Waveform type is LFM with deramping on receive. Platform and scene geometry is as defined in Figure 2.2.

Radar system parameters are given in Table 3.1. The scene size is 200×200 m when a sinc antenna pattern with $5°$ beamwidth is used. Point target simulator is able to generate IRF of multiple targets. Target position, velocity and acceleration compo-

Table 3.1: Moving Target Focusing Simulation System Parameters

Frequency	X band
Integration time	5 s
Pulse width	1 μs
Platform velocity (Y)	100 m/s
Noise figure	2 dB
Platform Initial Position (X)	10 km
Platform Initial Position (Y)	-250 m
Platform Initial Position (Z)	10000 ft

nents can be defined independently in cartesian coordinates. To observe the effects of more severe nonlinear target motion, a simplified human walking micro Doppler model is incorporated into the cross track motion model of the target. The micro Doppler model used is based on the detailed human locomotion model of Boulic [38]. This simplified model considers only torso and two legs as contributors of the micro Doppler since torso has the most prominent signature and arms and legs are assumed to have in phase cyclic signatures with arms having smaller contribution to the RCS [14].

Variation in range due to foot induced micro Doppler is given as [14]:

$$R_{foot}(t) = F_c L_c \left(t + \frac{\sin(2\pi F_c t + \phi_{foot})}{2\pi F_c} \right) + R_0, \tag{3.43}$$

where F_c is the cycle frequency which is the inverse of the time between two heel strikes of the same leg. L_c is the distance between two heel strikes of the same leg. ϕ_{foot} is the initial phase of the leg in the locomotion cycle. R_0 is the initial range.

Variation in range due to torso induced micro Doppler is given as [14]:

$$R_{torso}(t) = F_c L_c t + \frac{A \sin(2\pi F_c t + \phi_{body})}{2\pi F_c} + R_0, \tag{3.44}$$

where ϕ_{body} is the initial phase of the torso in the locomotion cycle. A is the amplitude of the forward-backward swing of the torso which is defined as:

$$A = -0.084s^2 + 0.084s, \tag{3.45}$$

where

$$s = F_c L_c. \tag{3.46}$$

In the simulation, ϕ_{foot} is $\pi/2$ radians for one leg and 0 radians for the other. ϕ_{body} is $\pi/4$ radians. F_c and L_c are set to 0.9 Hz and 1.9 m. These values are determined experimentally by [38] and [14]. The micro Doppler signature then becomes:

$$\mu_{bodypart}(t) = R_{bodypart}(t)v' - R_0, \tag{3.47}$$

where body part refers either torso or legs. v' is the target velocity direction. Micro Doppler signature is then added to the target position given in equation 3.18. Torso and leg micro Doppler variations are given in Figure 3.6.
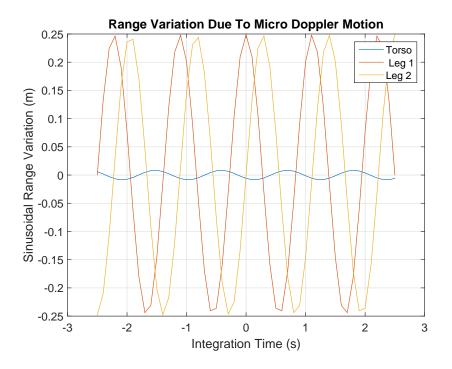

Figure 3.6: Micro Doppler Effect on Range Variation

Figure 3.7 shows IRFs for 5 different targets. Target parameters are given in Table 3.2.

Target no 5 has initial position at (-30, 40, 0) with 1.5 m/s cross track velocity and experiences micro Doppler torso motion in cross track direction. Such a non-linear motion component has no explicit form of along track smearing contribution yet experimental results show $\sim$70 m azimuth smearing. Note that smearing resulting from

33

Table 3.2: Moving Target Focusing Simulation Target Parameters

Parameter	Target No 1	Target No 2	Target No 3	Target No 4	Target No 5
Initial Position (X,Y,Z)	(0, 0, 0)	(10, -10, 0)	(40, 30, 0)	(-20, 20, 0)	(-30, 40, 0)
Velocity (X,Y,Z)	(0, 0, 0)	(1.2, 0, 0)	(0, 1.2, 0)	(1.2, 0, 0)	(1.2, 0, 0)
Acceleration (X,Y,Z)	(0, 0, 0)	(0, 0, 0)	(0, 0, 0)	(0.2, 0, 0)	(0, 0, 0)
RCS	1	1	1	1	1
MicroDoppler	No	No	No	No	Yes
Residual Range Migration	0 m	~1.15 m	~0.02 m	~1.05 m	~1.15 m
Along Track Smear	0 m	~0.26 m	~12 m	~100.6 m	N/A
Along Track Displacement	0 m	~125 m	0 m	~125 m	~125 m

micro Doppler shows a different signature from target velocity or acceleration induced smearing which supports the sinusoidal range variation effect of micro Doppler. It is shown in Figure 3.7 that cross track acceleration has more prominent effect on along track smearing than along track velocity of the target. The other point should be noted that small cross track velocity of the target may result in large along track displacements. This can impose a restriction on the minimum imaging area coverage not to have the target signature falling beyond the imaging scene.

3.3.2.2   Performance of Focusing Method on Point Target Simulator

Moving target focusing with 1.2 m/s along track target velocity is realized in the image formation part of the simulation. Results are shown in Figure 3.9. The point target SAR simulation target parameters are given in Table 3.3:

It is shown that Target 3 signature is focused successfully while Target 4 and 5 still have defocused signatures due to their non-linear motion components contributing the smear. Target 1 and 2 which are focused on the original image now have defocused signatures as expected since image formation is realized with an equivalent platform velocity according to equation 3.7.

Another simulation is run to analyze the target signature for a target which has both velocity components. Target parameters are given in Table 3.4.

Moving target focusing with 1.2 m/s along track velocity results given in Figure 3.11
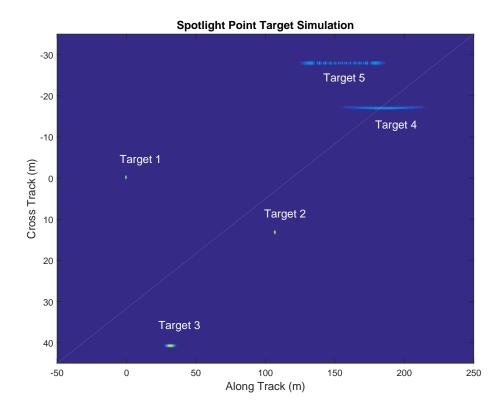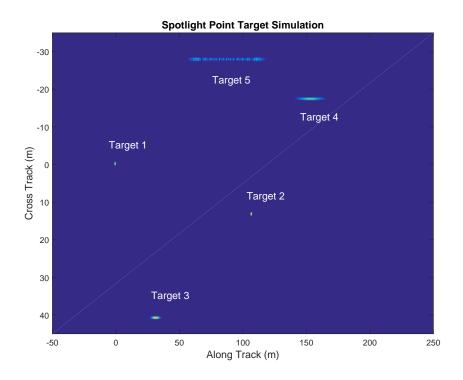
Figure 3.7: Point Target SAR Simulator

Table 3.3: Moving Target Focusing Simulation Set 1

Parameter	Target No 1	Target No 2	Target No 3	Target No 4	Target No 5
Initial Position (X, Y, Z)	(0, 0, 0)	(10, -10, 0)	(40, 30, 0)	(-20, 20, 0)	(-30, -30, 0)
Velocity (X, Y, Z)	(0, 0, 0)	(1.2, 0, 0)	(0, 1.2, 0)	(1.2, 0, 0)	(1.2, 0, 0)
Acceleration (X, Y, Z)	(0, 0, 0)	(0, 0, 0)	(0, 0, 0)	(0.07, 0, 0)	(0, 0, 0)
RCS	1	1	1	1	1
MicroDoppler	No	No	No	No	Yes
Residual Range Migration	0 m	~1.15 m	~0.02 m	~1.12 m	~1.15 m
Along Track Smear	0 m	~0.26 m	~12 m	~35.4 m	N/A
Along Track Displacement	0 m	~125 m	0 m	~125 m	~125 m

Figure 3.8: Point Target SAR Simulation Set 1

Figure 3.9: Moving Target Focusing Result of Set 1

Table 3.4: Moving Target Focusing Simulation Set 2

Parameter	Target No 1	Target No 2	Target No 3	Target No 4
Initial Position (X, Y, Z)	(0, 0, 0)	(10, -10, 0)	(40, 30, 0)	(-20, 20, 0)
Velocity (X, Y, Z)	(0, 0, 0)	(1.2, 0, 0)	(0.7, 1.2, 0)	(0.7, 1.2, 0)
Acceleration (X, Y, Z)	(0, 0, 0)	(0, 0, 0)	(0, 0, 0)	(0.2, 0, 0)
RCS	1	1	1	1
Micro Doppler	No	No	No	No
Residual Range Migration	0 m	~1.15 m	~0.63 m	~0.53 m
Along Track Smear	0 m	~0.26 m	~12 m	~112 m
Along Track Displacement	0 m	~125 m	~73 m	~73 m

show that Target 3 signature which has both along track smear and displacement on the original image is focused successfully at the displaced location.

In order to see the sensitivity of the method to the equivalent platform velocity choice a final simulation is run with the parameters given in Table 3.5.

Table 3.5: Moving Target Focusing Simulation Set 3

Parameter	Target No 1	Target No 2	Target No 3	Target No 4
Initial Position (X, Y, Z)	(0, 0, 0)	(10, -10, 0)	(40, 30, 0)	(-20, 20, 0)
Velocity (X, Y, Z)	(0, 0, 0)	(0, 1, 0)	(0, 1.2, 0)	(0, 1.6, 0)
Acceleration (X, Y, Z)	(0, 0, 0)	(0, 0, 0)	(0, 0, 0)	(0, 0, 0)
RCS	1	1	1	1
Micro Doppler	No	No	No	No
Residual Range Migration	0 m	~0.014 m	~0.02 m	~0.02 m
Along Track Smear	0 m	~10 m	~12 m	~16 m
Along Track Displacement	0 m	0 m	0 m	0 m

Moving target focusing with 1.2 m/s along track velocity results given in Figure 3.13 show that as the target velocity gets closer to the applied target velocity filter, its signature becomes well focused. This result is in line with the equivalent platform velocity related arguments given in section 3.3.
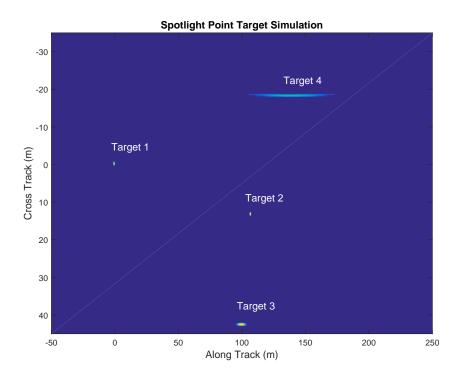
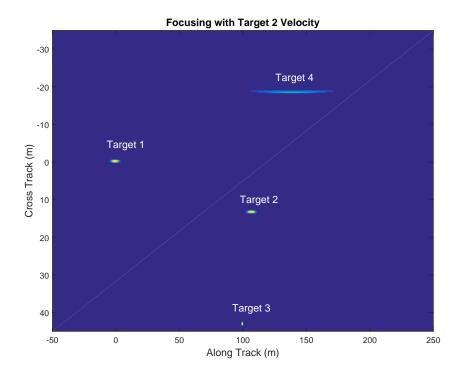Figure 3.10: Point Target SAR Simulation Set 2

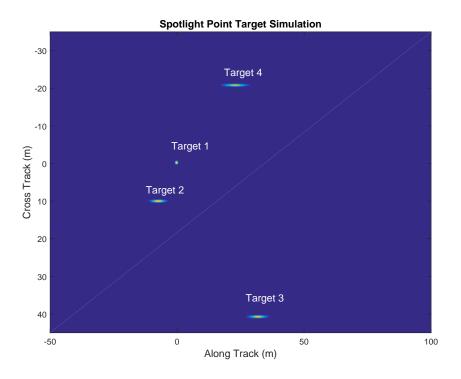Figure 3.11: Moving Target Focusing Result of Set 2

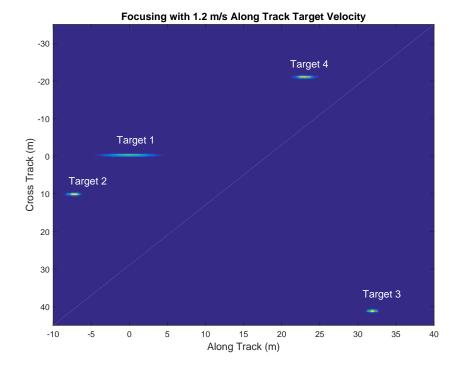Figure 3.12: Point Target SAR Simulation Set 3

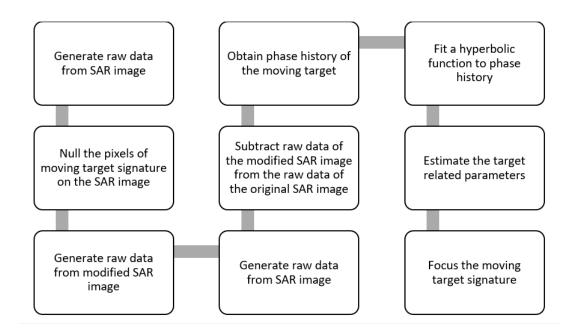Figure 3.13: Moving Target Focusing Result of Set 3

Figure 3.14: SAR Image Moving Target Focusing Approach

3.3.3 Conclusion

Point target focusing trials have demonstrated that target motion parameters are in close relationship with the target signature appeared on the SAR image. This leads us to offer a moving target focusing solution to the complete SAR image based on the extraction of the moving target phase history from the target signature. Phase history for each scatterer on the scene is formed by the relative range of the target which is determined by both target and platform motion parameters as it is discussed in the previous sections. Therefore, extracting the target range history should enable us to estimate some of the target motion parameters. After target motion parameters are estimated, they can be used to focus the smeared moving target signature on the image. However, extracting the range history of the target from a focused SAR image is not an easy task. Fully formed SAR image includes many scatterers which contribute to the image pixels other than the moving target of interest. In the scope of this thesis, a moving target range history extraction method is studied where the algorithm flow is given in Figure 3.14. Nevertheless, the method does not give successful results due to the sensitivity to the parameter estimation which is further explained below.

Generating raw data from the SAR image requires platform motion parameters (such as velocity, location etc.) and radar system parameters (such as transmit frequency, bandwith, resolution, coverage, pulse duration, sampling rate, antenna pattern, waveform type etc.) to simulate the received signal from the scene. This process of raw data conversion is based on the most basic idea of the SAR image formation: Each scatterer on the scene has a unique range history which is determined by the platform and scatterer geometry. To this end, each pixel of the SAR image is handled as an individual scatterer on the scene whose RCS corresponds to the pixel intensity and position on the scene is deduced from the pixel number, image coverage and resolution. Once the scatterer map is formed, transmit waveform is replicated with the system parameters of the SAR image. The last step of raw data generation is to determine the time delay and magnitude scale of the transmitted waveform for each scatterer. Relative range to the platform is calculated for each scatterer to obtain the time delay. Magnitude scale is obtained from both the antenna pattern and the pixel intensities. After the received waveform is generated according to equation 2.19, the raw data matrix is formed.

Target signatures, although smeared throughout the along track direction, have abrupt pixel intensity changes at the transitions with the background pixels. This makes it possible to replace the target containing pixel intensity values with 0 by visual inspection. Modified SAR image without any moving targets actually contains only the clutter pixels for the purpose of moving target detection. Similar to original SAR image, modified SAR image is converted to raw data with the same processing.

By subtracting raw data from each other, raw data of the moving target is aimed to be isolated from the image. The obtained target raw data can be processed with any generic SAR image formation algorithms to form a SAR image contanining only the moving target. The aim here on the other hand, is to obtain the phase history of the target which relates the target motion parameters to the target signature on the image as described in Displacement Effects and Smearing Effects section. The described raw data generation method uses the SAR image pixel intensities to represent the scatterers on the illuminated scene. However, this model does not adequately represent the dependency of the scatterer reflectivity to the aspect angle of the illuminating platform. This suggests that a higher precision raw data model is required to com-

pensate the lack of numerical precision encountered while subtracting the raw data results. Thus, no further results will be presented regarding this study.

If the described method were successful, moving target focusing could be implemented by estimating the target parameters from the data without assuming a range of parameter values for focusing. In that case, nulling the target signature on the SAR image could be automatized by simple pre-processing of the image to detect line-like signatures. Based on this idea, a second method is proposed for the moving target detection from SAR image by utilizing the physical appearence of the target signature on the image without needing any target motion parameters.

CHAPTER 4

SLOW MOVING TARGET DETECTION ON SAR IMAGES BY DYNAMIC PROGRAMMING

In this chapter, a dynamic programming based approach is proposed to detect slow moving, low reflectivity targets for airborne radar systems. This approach does not require any target related parameters which distinguishes the method from others in the literature. Main idea behind the approach stems from the answer to the question of what if we have only a SAR image at our hand without any knowledge of the data collection and image formation phases, is it possible to detect the moving targets on the image? The answer lies behind the most significant feature of the moving targets: their line-like signatures on the SAR image. As it is discussed in the previous chapter, moving targets experience displacement, smearing and residual range migration depending on the motion parameters. A typical slow moving target on the ground has both components (cross track and along track) of the velocity and acceleration. Therefore, its signature resembles a line structure on the SAR image. This suggests that detecting line-like features from the image may lead to successful detection of moving targets. To this end, template matching and Hough transform based methods are studied where both of them turn out to be insufficient to track the moving target signature due to the speckled nature of the SAR image. Speckle noise is an inherent and signal dependent phenomenon in SAR images which is caused by the phase fluctuations of the echo. This noise results in a high rate of false alarms and frequent target miss in both template matching and Hough transform based approaches. These trials suggested that a more sophisticated method, such as dynamic programming, which utilizes the physical features of the moving target signature may lead to successful results.

The proposed method in this chapter utilizes the reflectivity amplitudes of the SAR image, possibly containing multiple slow moving targets, and poses the target detection problem as a maximum likelihood sequence detection problem. Dynamic programming is applied to capture the target related features such as along track smeared target signatures in the SAR image to this aim. Typical clutter and target models are estimated from SAR images. First, the problem formulation is given and then the performance of the algorithm is illustrated on a real SAR image acquired with SARPER™ radar developed by ASELSAN.

4.1 Dynamic Programming Basics for Implementation on SAR Images

The dynamic programming based approach for slow moving target detection on a SAR image is closely related with the dim target detection problem, a problem also known as track-before-detect (TBD) problem. The goal is to adapt the sequence detection problem, whose solution is obtained via dynamic programming in general, to the problem of interest. At the outset, we would like to remind that SAR images are constructed with the processing of raw data whose duration is orders of magnitude larger than a typical coherent processing interval (CPI) of a GMTI system. Hence, a SAR image can be considered to contain sufficiently large energy return from the target, which is, unfortunately, not localized due to the target motion. The main goal of the study is to treat the problem as a sequence detection problem and utilize the track-before-detect methods to extract the target signal from the real-valued SAR image.

The main issues with DP-TBD algorithm are the partitioning of the target space, heavy computational load and storing multiple scans of data for processing [39]. The advantages of using a SAR image that reduce these problems in DP-TBD algorithms are:

- The use of a SAR image eliminates the problem of storing processed data since all of the information from the target is already stored in the SAR image,

- As the resolution increases the clutter to target return ratio decreases,

44

- Smeared moving target signature shows similar pixel intensities throughout the target containing pixels.

The features of the slow moving target signature on a SAR image are analyzed in Chapter 3. It is shown that moving target's signature experiences smearing and displacement mainly in along track direction due to the target motion. The prior knowledge regarding this line-like signature can be exploited to formulate a dynamic programming based solution for the detection of moving targets in the SAR images. This knowledge can be considered into two parts: prior knowledge of the continuity and prior knowledge of the physical appearance of lines [40]. The first part forms the ground for the Markov Random Field (MRF) target state model since the presence of neighboring pixels provides sufficient evidence for the presence of a line pixel. In other words, continuity of the line suggests that the presence of a line pixel is independent of the rest of the image pixels given the neighboring pixels. The second part indicates that the line structure is composed of pixels with similar intensity values such that Bayes' theorem of posterior conditional PDFs can be used to express the line structure where physical appearance of the lines is the given information.

For a more thorough understanding of the following problem formulation, the use of MRF needs to be elaborated. Markov model is a tool to represent the probabilistic SAR image model that characterizes spatial correlation in the SAR image under speckle noise. The different patches in the image can be considered as the conditionally dependent outputs of different filters. The variables of the Markov model have conditional dependencies. Hence, Markov model can be employed to model the texture in the SAR image. The main assumption behind this model is that current state is only dependent on the previous state. To this end, target states are modelled as Markov random walk since the presence of a pixel in a textured patch is dependent on some of the surrounding pixels rather than the rest of the image. Markov models are also used to fit a model to the instantaneous and time varying variations in signal features.

DP-TBD algorithm searches for the trajectory with the maximum score,i.e. logarithmic ratio of the posteriori probabilities, iteratively [41]. At each iteration, the path which maximizes the sum of the inherited score from the previous state and the state

transition cost is chosen. A state transition cost is assigned to each allowed state transition. Maximization process is realized only for the allowable states at each frame which makes DP more computationally efficient than the exhaustive search. At the end of the search, detection is made by thresholding the scores of each cell. Once a detection is made, trajectories can be traced backwards from the stored optimum state transition values as the name "Track Before Detect" suggests [42].

The details of DP algorithm can be found in [42]. Here, we present only the end result. The unobservable target states are modelled as a MRF where the presence of a pixel only depends on the pixels within a small neighboring region. Let us define the target state sequence as $(j_k \; j_{k-1} \ldots . . j_1)$ which is a MRF:

$$P(j_k|j_{k-1}j_{k-2}\ldots j_1) = P(j_k|j_{k-1}), \tag{4.1}$$

where j_k denotes the target state cell at time k. Then the ratio of the posteriori probabilities is given as a measure of target track score:

$$\log\left(\frac{P_{k|k}(H_1|Y_k)}{P_{k|k}(H_0|Y_k)}\right) = \log\left(\frac{P_{k|k}(j_kj_{k-1}\ldots j_1|Y_k)}{P_{k|k}(H_0|Y_k)}\right), \tag{4.2}$$

where Y_k denotes the measurement set $(y_k \; y_{k-1}\ldots.y_1)$ [42]. In our case, measurements are represented by the intensity values of the SAR image pixels. H_1 and H_0 denote target present and target not present cases, respectively. Bayes' theorem and MRF target state model are used as follows:

$$\frac{P_{k|k}(j_kj_{k-1}\ldots.j_1|Y_k)}{P_{k|k}(H_0|Y_k)} = \frac{P_{k|k}(Y_k|j_kj_{k-1}\ldots.j_1)}{P_{k|k}(Y_k|H_0)}\frac{p(H_1)}{p(H_0)}, \tag{4.3}$$

$$\frac{P_{k|k}(j_kj_{k-1}\ldots.j_1|Y_k)}{P_{k|k}(H_0|Y_k)} = \frac{p(y_k|j_k)}{p(y_k|H_0)}\frac{P_{k-1|k}(Y_{k-1}|j_kj_{k-1}\ldots.j_1)}{P_{k-1|k}(Y_{k-1}|H_0)}\frac{p(H_1)}{p(H_0)}, \tag{4.4}$$

$$\frac{P_{k|k}(j_kj_{k-1}\ldots.j_1|Y_k)}{P_{k|k}(H_0|Y_k)} = \frac{p(y_k|j_k)}{p(y_k|H_0)}\frac{P_{k|k-1}(j_kj_{k-1}\ldots.j_1|Y_{k-1})}{P_{k|k-1}(H_0|Y_{k-1})}, \tag{4.5}$$

where $P_{k|k-1}$ is the prior probability of the target states $(j_k \; j_{k-1}\ldots.j_1)$ and H_0 at time index k conditioned on the measurements up to the previous state and $p(y_k|j_k)$ and $p(y_k|H_0)$ denote probability density functions (pdf) of the conditioned measurements at time k [42]. Then conditional probability definition is applied as follows [42]:

$$P_{k|k-1}(j_kj_{k-1}\ldots j_1|Y_{k-1}) = P(j_k|j_{k-1}\ldots j_1)P_{k-1|k-1}(j_{k-1}j_{k-2}\ldots.j_1|Y_{k-1}), \tag{4.6}$$

Substituting equation 4.5 and equation 4.6 into equation 4.2 and applying the MRF model of target state sequence give:

$$\log\left(\frac{P_{k|k}(H_1|Y_k)}{P_{k|k}(H_0|Y_k)}\right) = \log\left(\frac{p(y_k|j_k)}{p(y_k|H_0)}P(j_k|j_{k-1})\frac{P_{k-1|k-1}(j_{k-1}j_{k-2}\ldots.j_1|Y_{k-1})}{P_{k-1|k-1}(H_0|Y_{k-1})}\right),$$
(4.7)

$$LPR_k(j_k) = \log\left(\frac{p(y_k|j_k)}{p(y_k|H_0)}\right) + \log(P(j_k|j_{k-1})) + LPR_{k-1}(j_{k-1}),$$
(4.8)

where LPR stands for the log probability ratio [42]. Dynamic programming solution from equation 4.8 is given as a recursive equation:

$$LPR_k^*(j_k) = l_k(j_k) + \max_{j_{k-1}}[\log(P(j_k|j_{k-1})) + LPR_{k-1}^*(j_{k-1})],$$
(4.9)

$$l_k(j_k) = \log\left(\frac{p(y_k|j_k)}{p(y_k|H_0)}\right),$$
(4.10)

where $LPR_k^*(j_k)$ is the score of the candidate track [42]. $l_k(j_k)$ is the log likelihood ratio of the target and the background intensity pdf models. Log likelihood ratio is independent of j_{k-1}. As a result, it can be taken outside the maximization. The term $P(j_k|j_{k-1})$ represents the transition cost function [42]. $LPR_{k-1}^*(j_{k-1})$ is the inherited track score from the previous stage. The illustration of the terms in equation 4.9 on an image matrix with dimensions $M \times N$ is given in Figure 4.1. The cell of interest is $LPR_k^*(3)$ whose allowed state transitions are within 2 pixels and denoted as $p(3|1:5)$. In Figure 4.1, k is omitted for simplicity from j_k expressions.

Target is declared when $LPR_k(j_k)$ score exceeds a threshold. Let the target state bins satisfying this criterion be shown as $j_{1:k}^*$. Operating only on $LPR_k^*(j_k)$ at each time index k makes DP computationally efficient. Tracing the target state trajectory back is possible once a detection is made. The detection threshold is commonly set by empirical methods. In this work, a detection is made by employing CFAR on the LPR scores. Employing CFAR after TBD is also studied by [43] for dim moving target detection from a sequence of infrared images.

SAR images have speckled texture inherently. Log-probability-ratio, LPR, is more robust for implementation than the probability ratio in heavily speckled image due to finite precision arithmetic problems [42].
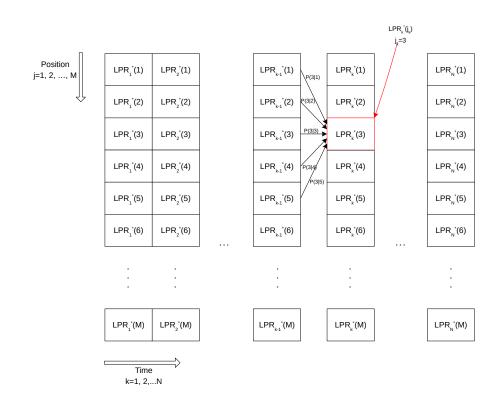
Figure 4.1: Dynamic Programming Illustration on The Image Matrix

4.2 Dynamic Programming Algorithm for Moving Target Detection on a SAR Image

Determining H_1 and H_0 hypotheses models forms the basis of the DP-TBD algorithm. The implementation illustrated in Figure 4.1 utilizes pixel intensities in each time column as target measurements. Therefore, features of the target present and target not present cases can be deduced from the corresponding pixel intensities.

Amplitude measurement models of H_1 and H_0 hypotheses used in this work are based on both a priori knowledge and test data observations. H_0 hypothesis model is determined as follows: Test image shown in Figure 4.2 is a high resolution heavily speckled SAR image. The speckle noise of this kind is best represented via multi parameter distributions to handle both contrast and mean intensity [44]. Different distributions are proposed in the literature in this sense such as log-normal, gamma, K-distribution [44], [45]. The best fit to the test data is achieved by a gamma distribution at our experiments. Homogeneous areas of the test SAR image determined by visual inspection are used to determine the best model fit with approximately 50000 sample pixels. Figures 4.2 and 4.3 show the distribution fitting results to the gamma distribution whose logarithm is given as,

$$\log(f_g(x|a,b)) = -a\log(b) - \log(\Gamma(a)) + (a-1)\log(x) - \frac{x}{b}, \qquad (4.11)$$

where a and b are the two parameters of the gamma distribution. $\Gamma(.)$ is the Gamma function. The distribution parameters, i.e., the fitted shape (a) and scale (b) parameters, are $a = 2.88$, $b = 0.50$ and $a = 2.68$, $b = 0.44$, for the clutter data samples collected from two different areas shown in Figure 4.2 and Figure 4.3, respectively.

Similar to the clutter intensity pdf estimation, the target intensity pdf can be estimated by considering cumulative behavior of the target containing cells. To this end, the signature of a moving target in the SAR image needs to be analyzed. The moving targets have line-like signatures in the SAR images due to phase errors resulting from uncompensated target motion. These errors smear and displace the target signature in along track direction [37], [46], [36]. The extents of the displacement and smearing depend on the target velocity and acceleration. The line-like trail smears also in the cross track direction due to the residual range migration of the target after the range
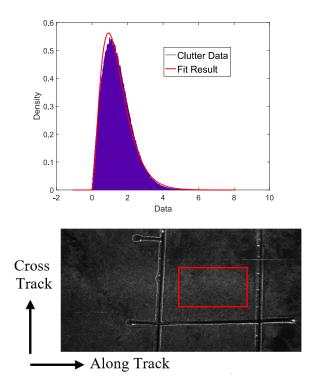
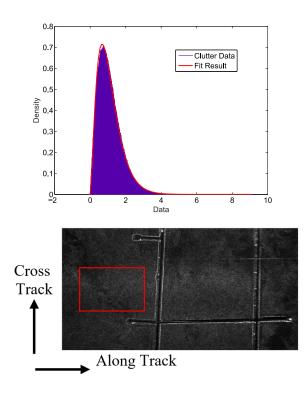Figure 4.2: Sample Area 1 and The Associated Intensity pdf

Figure 4.3: Sample Area 2 and The Associated Intensity pdf

migration correction. The extent of the smear in the cross track direction is much shorter than that in the along track direction which constitutes the line-like-form.

A priori knowledge of the expected line-like rectangular shaped target signature in the SAR image is used to build the target intensity model. The expected signature is nearly a rectangle whose width is within 3-10 pixels (in rows) and length is within 100-300 pixels (in columns) in the tested SAR image. The pixel intensities within this rectangle show slow variation. Transitions between background and target pixels are visible on the image which means that pixel intensities abruptly change at the transitions. Therefore, as a target intensity model Gaussian pdf with a small variance about the mean corresponding to the average target pixel intensity is used.

The logarithm of Gaussian pdf is given as:

$$\log(f_n(x|\mu,\sigma)) = -\frac{\log(2\pi\sigma^2)}{2} - \frac{(x-\mu)^2}{2\sigma^2}, \tag{4.12}$$

where μ and σ are the mean and standard deviation parameters of the normal distribution, respectively.

The optimum width of the rectangular target model deduced from the data is 5 pixels considering the smear in the cross track direction. Hence log likelihood ratio of the cell j_k is constructed from pixel intensities Y_k of the pixels $\{j_k - 2, j_k, j_k + 2\}$ as follows:

$$l_k(j_k) = \begin{cases} H_0 : \log(f_c(Y_k(j_k + 2))f_c(Y_k(j_k))f_c(Y_k(j_k - 2))) \\ H_1 : \log(f_c(Y_k(j_k + 2))f_t(Y_k(j_k))f_c(Y_k(j_k - 2))) \end{cases}, \tag{4.13}$$

where $f_c(\cdot)$ denotes clutter intensity pdf and $f_t(\cdot)$ denotes target intensity pdf. This model takes into account that the searched trajectory is line-like and allowable transitions are up to 2 pixels. Enforcing background intensity pdf models to the cells which are two pixels apart from the test cell ensures that line-like signature of the target is traced with minimum deviations in the range direction. The likelihood of hypothesis H_1 in equation 4.13 becomes large if the intensity of the cell of interest fits the target intensity pdf while the intensities of the cells which are 2 pixels apart fit the clutter intensity pdf. H_0 hypothesis, on the other hand, requires that both the cell of interest and the cells which are 2 pixels apart fit the clutter intensity pdf.

The smear in the cross track direction of the target signature is also used to determine the transition pdf. Transition pdf is assigned considering the expected trajectory of the target in the image, i.e., line-like signature. Therefore, no transitions are allowed between image cells which are more than 2 pixels apart as illustrated in Figure 4.1. The transition pdf used in this work is determined as:

$$P(j_k|j_{k-1}) = \begin{cases} \alpha, & j_k - j_{k-1} = 0 \\ \beta, & j_k - j_{k-1} = \mp 1 \\ \gamma, & j_k - j_{k-1} = \mp 2 \\ 0, & \text{otherwise} \end{cases}, \tag{4.14}$$

where $\gamma < \beta < \alpha$. These values in the transition pdf ensure that the transition to the cell in the same row is the most likely while the likelihood decreases with the distance. Note that the transition to a cell which is more than 2 pixels apart is not allowed. Restrictive transition costs (assigning zero probability for some transitions) are applicable when the target trajectory has deterministic restrictions, as in moving target signatures in the SAR images [41].

Due to the possibility of multiple targets in the SAR image, we introduce modifications in equation 4.9. Transitions between target pixels and background pixels have a serious effect on the LPR values. The long trail of the target signature in the along track direction (time) causes gradual accumulation of LPR towards the end of the trail. When the target signature is over, the accumulated likelihood ratio cannot decay sufficiently rapidly in time resulting in clutter pixels having high LPR values which might exceed the threshold. To reduce the accumulation of LPR values, a forgetting factor, $0 < \lambda < 1$, is introduced as follows:

$$LPR_k^*(j_k) = l_k(j_k) + \lambda \max_{j_{k-1}}[\log(P(j_k|j_{k-1}) + LPR_{k-1}^*(j_{k-1})], \tag{4.15}$$

where the maximum of the prior state score is weighted with the factor λ so that past LPR values are forgotten. Furthermore, to prevent LPR values from getting too large during iterations, when LPR values exceed a threshold η it is reset to $\eta > 0$. Similarly, LPR values might become very low throughout the consecutive background pixels. This may cause a delay in target detection when a switch occurs from background pixels to target pixels. To overcome this, LPR is limited from below to $-\eta$. As a result, LPR values are hard-limited to interval $[-\eta, \eta]$.

The pseudocode of the proposed algorithm is given below. The parameter definitions are in line with the matrix representation of the SAR image, whose dimensions are $M \times N$, as given in Figure 4.1. The goal is to calculate the LPR scores of all pixels of the image by using pixel intensities as measurements, Y_k.

Algorithm 1 Calculate $LPR_k(j_k)$

Require: $LPR_1(j_1) = 0$ for $j = 1 : M$

  for $k = 2 : N$ **do**

    for $j = 3 : M - 2$ **do**

      $H_0 \leftarrow \log(f_c(Y_k(j_k + 2))f_c(Y_k(j_k))f_c(Y_k(j_k - 2)))$

      $H_1 \leftarrow \log(f_c(Y_k(j_k + 2))f_t(Y_k(j_k))f_c(Y_k(j_k - 2)))$

      $l_k(j_k) \leftarrow H_1 - H_0$

      $temp \leftarrow \max(LPR_{k-1}(j_{k-1} - 2) + \log(\gamma),\ LPR_{k-1}(j_{k-1} - 1) + \log(\beta),$
      $LPR_{k-1}(j_{k-1}) + \log(\alpha),\ LPR_{k-1}(j_{k-1} + 1) + \log(\beta),\ LPR_{k-1}(j_{k-1} + 2) +$
      $\log(\gamma))$

      $LPR_k(j_k) \leftarrow l_k(j_k) + \lambda \times temp$

      if $LPR_k(j_k) \leq -\eta$ **then**

        $LPR_k(j_k) = -\eta$

      else if $LPR_k(j_k)gt\eta$ **then**

        $LPR_k(j_k) = \eta$

      end if

    end for

  end for

State transition diagram of the algorithm is given in Figure 4.4. The state transition diagram is a directed, acyclic and layered graph with layers $k = 1 : N$. Each layer has $j = 1 : M$ nodes as states. It can be seen that each state has 5 predecessors. Therefore, for each node, it is required to store the state transition costs up to 5 predecessors. The complexity of the algorithm is determined by the number of arcs in the state transition diagram. The algorithm has $O(5MN)$ complexity which makes it more efficient than the exhaustive search of the same size input with $O(M^N)$ complexity.

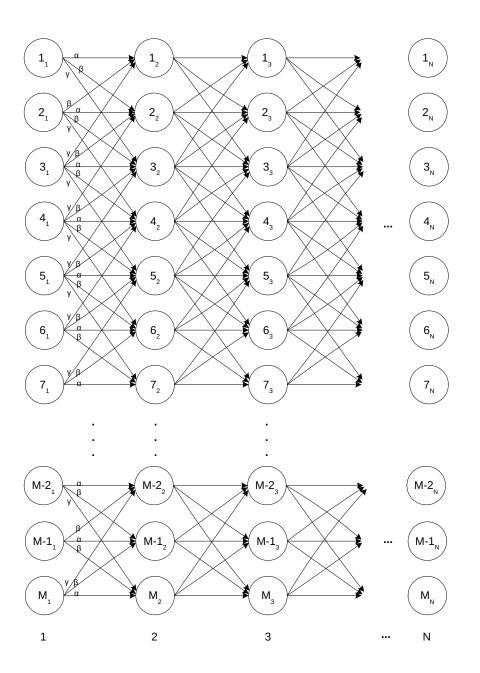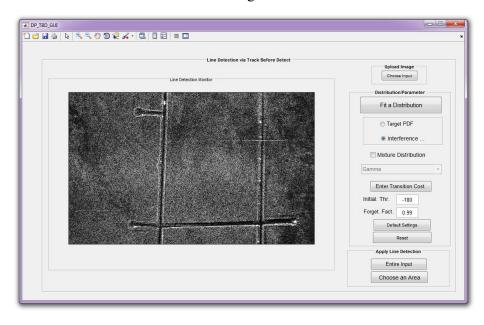Figure 4.4: DP-TBD State Transition Diagram

4.3 Results of Dynamic Programming Method

To ease the implementation of the DP-TBD method, a Graphical User Interface (GUI) model is constructed in MATLAB$^{\text{TM}}$ environment. The details regarding the user interface are given in the following section. The method's performance is illustrated on both simulation data and real test data respectively via the GUI model.

4.3.1 Graphical User Interface Development for Dynamic Programming

The DP-TBD GUI interface is shown in Figure 4.5.

Figure 4.5: DP TBD User Interface

The DP-TBD GUI consists of three main windows: upload image, distribution/parameter settings and line detection. The first part enables the user to select a test image from a predefined directory. The test image can be in either double or complex valued form. The image matrix has range cells as rows and cross range cells (along track cells) as columns. The distribution/parameter settings part aids to define hypotheses models, transition cost vector, forgetting factor and initialization threshold for the test image. In this window, "Fit a Distribution" button provides distribution fitting results of a user selected area from the image. The avaliable distribution mod-
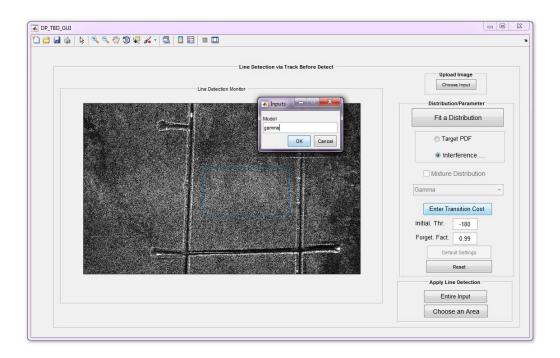
Figure 4.6: DP TBD Select an Area to Fit a Distribution

els are as follows: normal, exponential, gamma and Rayleigh. The user selects an area on the image after pressing the Fit Distribution button and chooses one of the avaliable distribution models. The process is illustrated on Figure 4.6 and Figure 4.7.

Hypotheses models can be entered directly via "Target PDF" and "Interference PDF" radio buttons for H_1 and H_0 hypotheses respectively. If the pdf model to be entered is a mixture pdf, "Mixture Distribution" checkbox needs to be selected before entering the model parameters. Otherwise, the program does not allow to enter a second pdf model for the same hypothesis. Mixture model selection is followed by a dialog box to define the corresponding weights of the included mixture models. This is shown in Figure 4.8. The distribution models can be selected from a drop-down list which is enabled only after one of the radio buttons is selected. In order to run the DP method on the test image, both hypotheses models need to be defined. An illustration of a interference pdf model definition is shown in Figure 4.9.

"Enter Transition Cost" button offers a dialog box to enter the transition cost vector of size 1×5. Transition cost vector field only accepts double values. Lastly, "Forgetting Factor" and "Initialization Threshold" buttons enable the user to define forgetting
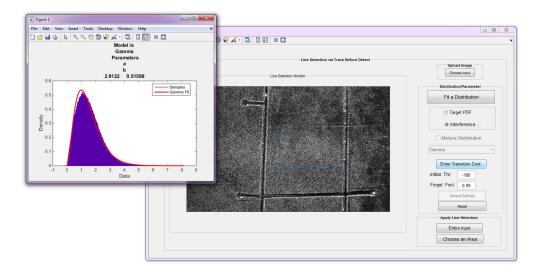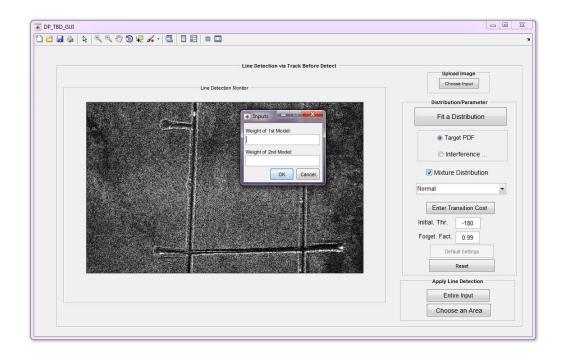
Figure 4.7: DP TBD Fit a Distribution

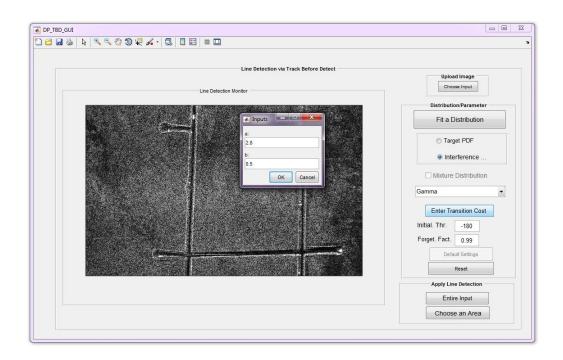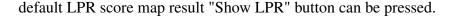Figure 4.8: DP TBD Mixture Model Weight Definition

Figure 4.9: DP TBD Interference Model

factor and initialization threshold for the test image. Both fields accept double values. Both of these parameters are mandatory for the algorithm to run. The "Default Settings" button at the end of the distribution/parameter settings window offers a default set for the mandatory distributions/parameters.

Finally, "Remove All Selections" button clears all the defined models and parameters except the input image selection.

Line detection window applies DP-TBD algorithm on the uploaded image with the parameters defined in distribution/parameter settings window. DP-TBD algorithm can be applied on the entire test image or a selected part of it using "Entire Input" and "Choose an Area" buttons respectively. As a result, LPR score surface map of the input is shown in the main scene.

Once a detection decision is made, 3 buttons which are named as "Show Detections", "Show Input" and "Show LPR" appear at the bottom of the main scene as shown in Figure 4.10. When "Show Detections" button is pressed, the algorithm runs CFAR detection process on the LPR score map. To see the input image,"Show Input" button can be pressed without losing the results of the existing scenario. To switch back the

default LPR score map result "Show LPR" button can be pressed.
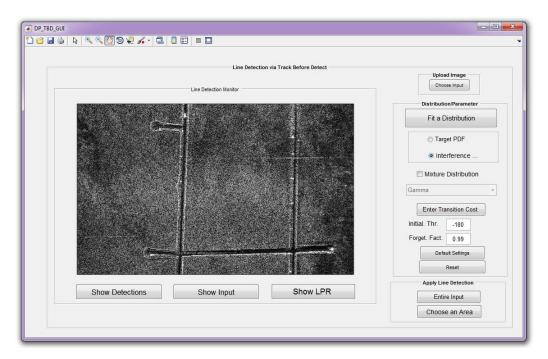

Figure 4.10: DP TBD Detection Page

4.3.2 Performance of Dynamic Programming Method on Simulation Data

Before moving on to the real data results, the algorithm is tested on simulated data. Four different targets with Gaussian pdf are modelled with additive normally distributed noise background to analyze the behavior of the algorithm. The parameters used in simulations are given in Table 4.1.

The target intensity pdf, transition pdf and forgetting factor are selected as the ones used in the real data. On the other hand, the background pdf model is selected as a normal distribution which is given in equation 4.12 with $\mu = 1$, $\sigma = 1$. The threshold η is adjusted considering the characteristics of the simulated data. Monte Carlo (MC) simulations are carried out 1000 times. In each MC run, noise and target realizations are obtained with the same density parameters. The two different realizations of the simulated data are shown in Figure 4.11.

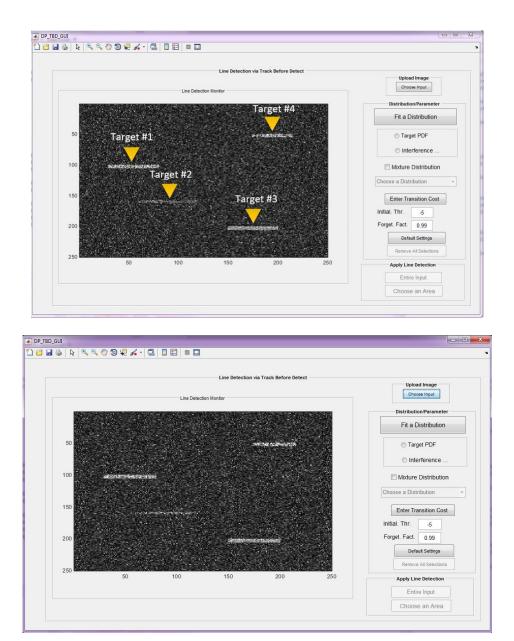In order to assess the effectiveness of the DP algorithm on simulation data with vary-

Figure 4.11: Simulated Data Realizations.

Table 4.1: Simulation Parameters

Parameter	Value	Description
$f_t(\cdot)$	$f_n(x\|4, \sqrt{2})$	Target intensity pdf
$f_c(\cdot)$	$f_n(x\|1, 1)$	Clutter intensity pdf
$P(j_k\|j_{k-1})$	α=0.9 β=0.05 γ= 0.001	Transition pdf
λ	0.99	Forgetting factor
η	5	Threshold

ing parameters, a measure of performance needs to be defined. Similar to classical detection problems, the performance of the method is measured via probability of detection and probability of false alarm rates which are defined as follows:

$$P_d = \frac{\text{number of detected target cells}}{\text{number of total target cells}}, \tag{4.16}$$

$$P_{fa} = \frac{\text{number of falsely detected target cells}}{\text{number of total clutter cells}}, \tag{4.17}$$

where P_d and P_{fa} denote probability of detection and probability of false alarm, respectively.

The simulated background data has dimensions of 250×250 pixels. Target signatures are modelled as 5×51 pixel sized vectors with Gaussian pdf with parameters given in Table 4.2. Main target to be detected is Target 1. Target 3 and 4 have slight mismatch to target intensity pdf model. Target 2 is the control target whose main purpose is to observe the effect of the severe target intensity pdf mismatch. Receiver operating characteristic curve is given in Figure 4.12 for Target 1. Other targets mismatching to target intensity pdf model are shown in the same figure for the sake of completeness.

Another set of simulations is carried out by changing background pdf $f_c(\cdot)$ parameters used by the DP algorithm to $\mu = 1$, $\sigma^2 = 2$ with the same Monte Carlo data-set (Hence there is a mismatch between the data and the parameters used in the DP algorithm). Receiver operating characteristic curve is given in Figure 4.13.

A final set of simulations is carried out by changing background pdf $f_c(\cdot)$ parameters

Table 4.2: Target Parameters

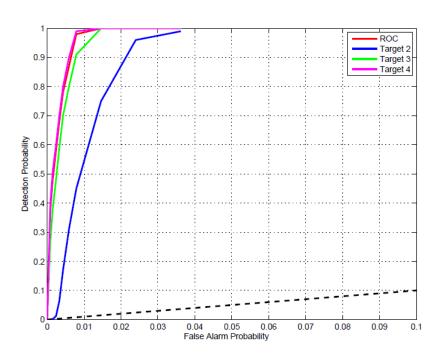| Target No	PDF Parameters
1	$\mu = 4 \,;\, \sigma^2 = 2$
2	$\mu = 2.5 \,;\, \sigma^2 = 2$
3	$\mu = 4 \,;\, \sigma^2 = 5$
4	$\mu = 4 \,;\, \sigma^2 = 1$

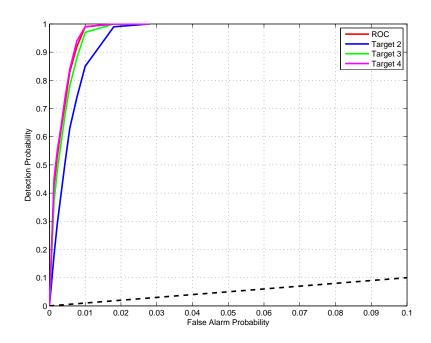Figure 4.12: Receiver Operating Characteristics for Synthetic Data.

Figure 4.13: ROC for Synthetic Data With Variance Mismatch.

used by the DP algorithm to $\mu = 2$, $\sigma = 1$ with the same Monte Carlo data-set, i.e., a mismatch in the mean value for the clutter hypothesis is created. Receiver operating characteristic curve is given in Figure 4.14.

The presented results show that the detection performance is heavily influenced by the target model mismatch. Figure 4.12 and Figure 4.13 show high probability of detection rates for Target 1, 3 and 4. The reason is that these targets are in good agreement with the target intensity pdf. Variance mismatch of the clutter intensity pdf results in higher false alarm rate than the case of no clutter intensity pdf model mismatch. Figure 4.14 shows lower detection probabilities for all targets as the clutter intensity pdf becomes similar to target intensity pdf. Target 2 has the lowest detection rate since the gap between the target intensity pdf and the clutter intensity pdf model is the smallest in this case.

As a result of this experiment we can conclude that if the parameters of H_1 is relatively close to the true target behavior and the background pdf is homogeneous throughout the image, the proposed approach is expected to give satisfactory results.
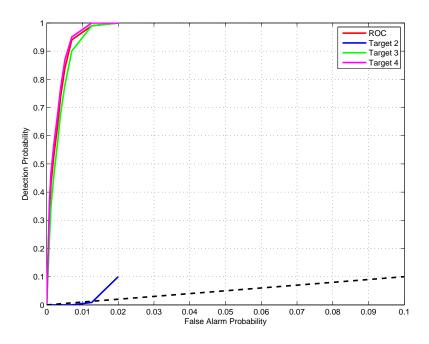
Figure 4.14: ROC for Synthetic Data With Mean Mismatch.

4.3.3 Performance of Dynamic Programming Method on Field Data

The DP-TBD algorithm is evaluated on real data collected from a manned platform carrying SARPER™ radar system. SARPER™ is an X band airborne radar system with slotted waveguide antenna [47]. Test image is a high resolution ($\ll$ 1 m) SAR image acquired at a range beyond 10 km. Test data include 3 controlled slow movers with approximately 1 m/s velocity. An example SAR image on which targets are marked is shown in Figure 4.15. Test site includes discrete clutter sources and road-soil boundaries.

Satellite image of the test site is given in Figure 4.16.

The proposed method is applied on an actual SAR image containing slow moving targets. The search of the targets is implemented via equation 4.12 on the test SAR image amplitude. The parameters used in this work are given in Table 4.3.

LPR score surface obtained is given in Figure 4.17. In the figure, it is shown that target LPR scores rise towards the center of the target signature and they gradually
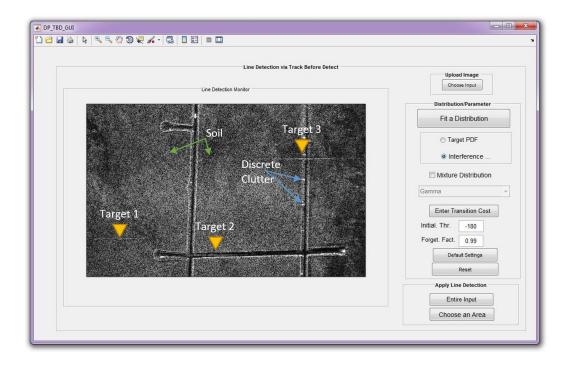
Figure 4.15: Test SAR Image Acquired with SARPER™

Figure 4.16: Satellite Image of the Test Site

Table 4.3: Parameters Utilized for the Field Experiment

Parameter	Value	Description
$f_t(\cdot)$	$f_n(x\|4,\sqrt{2})$	Target intensity pdf
$f_c(\cdot)$	$f_g(x\|2.8,0.5)$	Clutter intensity pdf
$P(j_k\|j_{k-1})$	α=0.9 β=0.05 γ= 0.001	Transition pdf
λ	0.99	Forgetting factor
η	180	Threshold

decrease towards the end as expected. Since the search is for the line-like trajectories in SAR image, some other similar segments of the image with the similar features, i.e., false alarms, are also captured.

To see the detections whose LPR scores exceed the threshold, a 2 dimensional CFAR filter is implemented. One dimensional guard cells and threshold cells in the conventional CFAR are replaced with cells in a rectangular form. Similar to the conventional method, a CFAR threshold is estimated from the neighboring cells. The illustration is given in Figure 4.18.

LPR scores after thresholding are shown in Figure 4.20 where detections are marked in green color. This shows that 3 controlled targets are detected with a few false alarms due to the line-like background features in the image.

Another SAR image acquired with SARPER$^{\text{TM}}$ radar system with 3 controlled slow movers with approximately 1 m/s velocity in the same test campaign is shown in Figure 4.21. The satellite image of the test site is shown in Figure 4.22. Test site includes different soil textures and road-soil boundaries. Background hypothesis pdf model is estimated from the SAR image by visually determining the target free sample area shown in Figure 4.23. The best fit gamma pdf model shown in Figure 4.23 has different parameters than the estimated background pdf model of the previous SAR image since the two have different soil texture characteristics.
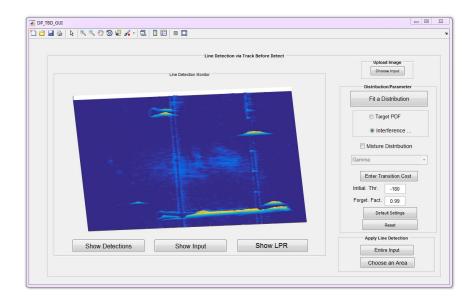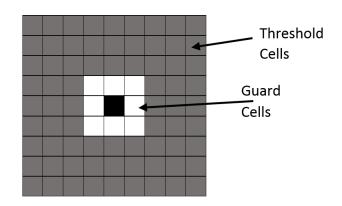
Figure 4.17: LPR Score Surface
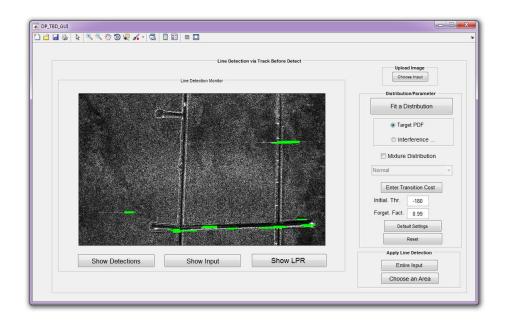

Figure 4.18: 2-D CFAR Illustration
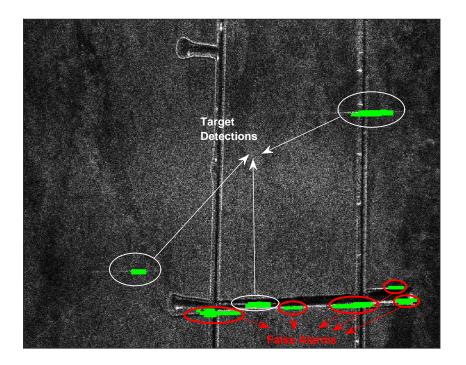
Figure 4.19: Detections of the First Test Image

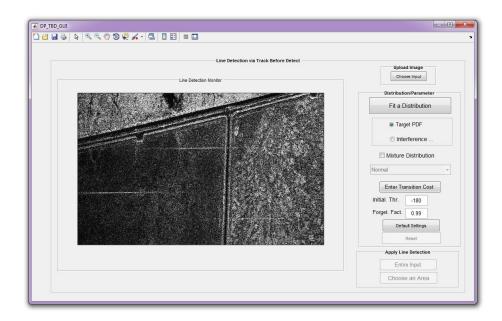Figure 4.20: LPR After Thresholding

Figure 4.21: Second Real Data Sample Image

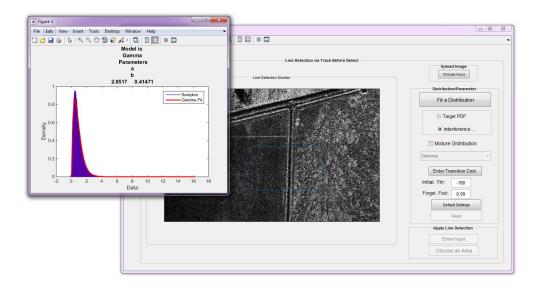Figure 4.22: Satellite Image of Second Test Site

Figure 4.23: Background PDF Model Estimation

The proposed method is implemented on this real SAR image sample with the algorithm parameters given in Table 4.4.

Table 4.4: Parameters Utilized for the Second Field Experiment

Parameter	Value	Description
$f_t(\cdot)$	$f_n(x\|4, \sqrt{2})$	Target intensity pdf
$f_c(\cdot)$	$f_g(x\|2, 0.5)$	Clutter intensity pdf
$P(j_k\|j_{k-1})$	α=0.9 β=0.05 γ= 0.001	Transition pdf
λ	0.99	Forgetting factor
η	180	Threshold

LPR score surface map is given in Figure 4.24. Results show triangular shaped LPR score accumulations for moving targets as expected. Different soil textures within the image show different LPR accumulation trends where some of them seem to cause false alarms. CFAR thresholding result of the LPR map is given in Figure 4.25. 3 moving targets are detected with a few false alarms denoted on the image given in Figure 4.26.

70

Figure 4.24: LPR Score Map of the Second Test Image
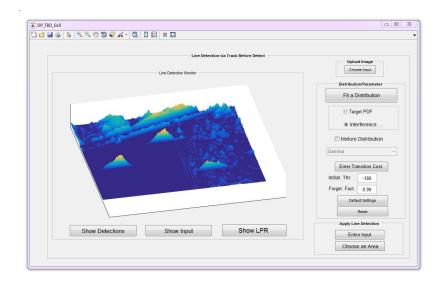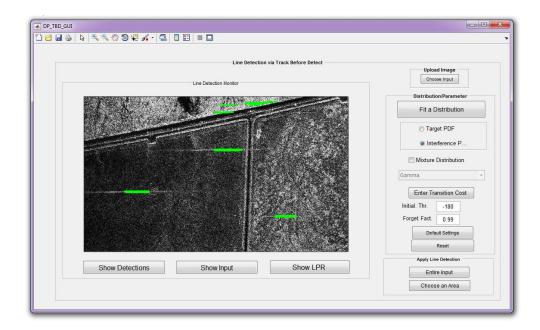

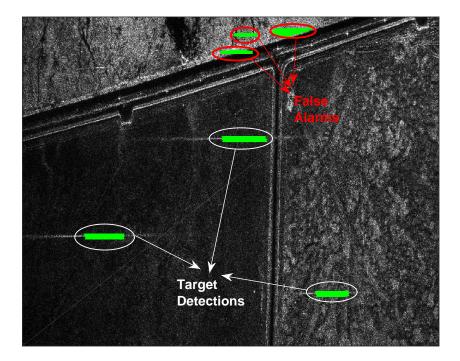Figure 4.25: Detections of the Second Test Image

Figure 4.26: LPR After Thresholding for the Second Test Image

Results of the proposed method implemented on two real SAR image samples demonstrate that the method holds the potential for detecting moving targets on a SAR image with no prior information/assumption of target motion or data collection system parameters.

CHAPTER 5

CONCLUSION

5.1 Thesis Summary

This work mainly focuses on moving target signature features in the SAR image and the utilization of these features to detect the slow moving targets from SAR images. The most prominent features of the moving target signature, i.e. smearing and displacement, stem from the target motion parameters. Both of the detection methods suggested in this thesis aim to detect slow moving targets from a SAR image but utilize different features of the moving target signature. The former one, i.e. moving target focusing method, requires target motion parameters to form the phase history of the moving target such that its smeared signature becomes focused. This method implemented successfully for point SAR targets. There are some illustrations of this method for the whole SAR image in the literature especially for foliage penetration radars. In this thesis, the method suggested for the whole image is based on generating the raw data model of the SAR image. However, this model turns out to be insufficient to represent the practical SAR data. Contrary to the focusing based method, the latter one, i.e. dynamic programming based method, does not require any target motion parameter estimation. Instead, the required data is extracted from the reflectivity amplitudes of the SAR image which makes this method more appealing for the cases where no input other than a focused SAR image is avaliable. The method has proven to be useful on both simulated and real SAR data containing multiple targets.

5.2 Future Work

Detection of moving targets from a SAR image is an intriguing problem since the characteristics of the SAR data have major impacts on the performance of the suggested method. Dynamic programming based approach holds the potential for detecting moving targets although it requires some of the image features to be estimated. As long as the accurate estimates of these features are provided, multiple moving targets can be detected from the SAR image without any prior knowledge of data collection or image formation processes.

These preliminary results of dynamic programming do not output any target related motion parameters such as target velocity and direction. Once the detection is made, the signature of the moving target can be used to estimate some of the target motion parameters.

Generally, applying moving target focusing methods to the whole SAR image without any prior knowledge of the target presence is computationally troublesome. The reason is that moving target focusing filters should include various target velocity alternatives to successfully focus the smeared target signatures. The preliminary results of the dynamic programming based method can be used as input to limit the areas on the image where focusing of the moving target signature method will be implemented.

In order to effectively operate in airborne platforms, DP-TBD based method can be implemented to Stripmap SAR with large coverage. However, degraded resolution of Stripmap SAR images with respect to Spotlight SAR affects the line-like appearance of moving target signatures on the image. Therefore, state transitions and hypotheses models need to be carefully constructed.

Field tests including more targets with different velocity and RCS parameters such as cars, tanks etc. should be carried out to assess the overall performance of DP-TBD based method more comprehensively for moving target detection on SAR images.

REFERENCES

[1] K. Y. Li, F. Uysal, S. U. Pillai, and L. J. Moore, "Modified space-time adaptive processing for dismount detection using synthetic aperture radar," in *2012 IEEE Radar Conference*, pp. 116–121, IEEE, 2012.

[2] M. McDonald and A. Damini, "Characterisation of dismounted combatants radar signature from airborne platforms," in *The 7th European Radar Conference*, pp. 45–48, IEEE, 2010.

[3] L. A. Gorham and L. J. Moore, "SAR image formation toolbox for MATLAB," in *Algorithms for Synthetic Aperture Radar Imagery XVII*, vol. 7699, p. 769906, International Society for Optics and Photonics, 2010.

[4] X. Mao, D.-Y. Zhu, and Z.-D. Zhu, "Signatures of moving target in polar format spotlight SAR image," *Progress In Electromagnetics Research*, vol. 92, pp. 47–64, 2009.

[5] W. Carrara, R. Goodman, and R. Majewski, *Spotlight Synthetic Aperture Radar: Signal Processing Algorithms,(ser. Artech House remote sensing library).* Norwood, MA, USA: Artech House, 1995.

[6] Yongkang Li, Tong Wang, Baochang Liu, and Ruixian Hu, "High-Resolution SAR Imaging of Ground Moving Targets Based on the Equivalent Range Equation," *IEEE Geoscience and Remote Sensing Letters*, vol. 12, no. 2, pp. 324–328, 2014.

[7] J. R. Fienup, "Detecting moving targets in SAR imagery by focusing," *IEEE Transactions on Aerospace and Electronic Systems*, vol. 37, no. 3, pp. 794–809, 2001.

[8] J. R. Fienup, "Phase error correction by shear averaging," *Signal Recovery and synthesis III*, vol. 4, 1989.

[9] R. A. Muller and A. Buffington, "Real-time correction of atmospherically degraded telescope images through image sharpening," *JOSA*, vol. 64, no. 9, pp. 1200–1210, 1974.

[10] J. S. Goldstein, M. L. Picciolo, M. Rangaswamy, and J. D. Griesbach, "Detection of dismounts using synthetic aperture radar," in *2010 IEEE Radar Conference*, pp. 209–214, IEEE, 2010.

[11] M. Newey, G. R. Benitz, D. J. Barrett, and S. Mishra, "Detection and Imaging of Moving Targets with LiMIT SAR Data," *IEEE Transactions on Geoscience and Remote Sensing*, vol. 56, no. 6, pp. 3499–3510, 2018.

[12] V. T. Vu, T. K. Sjogren, M. I. Pettersson, A. Gustavsson, and L. M. H. Ulander, "Detection of moving targets by focusing in UWB SAR—Theory and experimental results," *IEEE Transactions on Geoscience and Remote sensing*, vol. 48, no. 10, pp. 3799–3815, 2010.

[13] V. C. Chen, *The micro-Doppler effect in radar*. Artech House, 2011.

[14] G. E. Smith, "Radar Target Micro-Doppler Signature Classification," 2008.

[15] O. R. Fogle and B. D. Rigling, "Micro-range/micro-Doppler decomposition of human radar signatures," *IEEE Transactions on Aerospace and Electronic Systems*, vol. 48, no. 4, pp. 3058–3072, 2012.

[16] B. Deng, H.-Q. Wang, X. Li, Y.-L. Qin, and J.-T. Wang, "Generalised likelihood ratio test detector for micro-motion targets in synthetic aperture radar raw signals," *IET Radar, Sonar & Navigation*, vol. 5, no. 5, pp. 528–535, 2011.

[17] O. R. Fogle and B. D. Rigling, "Dismount feature extraction from circular synthetic aperture radar data," in *2012 IEEE Radar Conference*, pp. 122–127, IEEE, 2012.

[18] N. Amrouche, A. Khenchaf, and D. Berkani, "Multiple target tracking using track before detect algorithm," in *2017 International Conference on Electromagnetics in Advanced Applications (ICEAA)*, pp. 692–695, IEEE, 2017.

[19] H. Yong and G. Jian, "A track-before-detect algorithm for statistical MIMO

radar multitarget detection," in *2010 IEEE Radar Conference*, pp. 12–16, IEEE, 2010.

[20] L. R. Moyer, J. Spak, and P. Lamanna, "A multi-dimensional Hough transform-based track-before-detect technique for detecting weak targets in strong clutter backgrounds," *IEEE Transactions on Aerospace and Electronic Systems*, vol. 47, no. 4, pp. 3062–3068, 2011.

[21] Z. Wang and J. Sun, "Maneuvering target tracking via dynamic-programming based Track-Before-Detect algorithm," in *2016 CIE International Conference on Radar (RADAR)*, pp. 1–4, IEEE, 2016.

[22] W. Yi, L. Kong, J. Yang, and X. Deng, "A tracking approach based on dynamic programming track-before-detect," in *2009 IEEE Radar Conference*, pp. 1–4, IEEE, 2009.

[23] F. Gao, F. Zhang, H. Zhu, J. Sun, and J. Wang, "An improved TBD algorithm based on dynamic programming for dim SAR target detection," in *2014 12th International Conference on Signal Processing (ICSP)*, pp. 1880–1884, IEEE, 2014.

[24] E. Kalender, "Parametric estimation of clutter autocorrelation matrix for ground moving target indication," Master's thesis, Middle East Technical University, 2013.

[25] E. Anadol, "A knowledge based approach in GMTI for the estimation of the clutter covariance matrix in space time adaptive processing," Master's thesis, Middle East Technical University, 2012.

[26] G. Yıldırım, "Antenna patterns for detecting slowly moving targets in two channel gmti processing," Master's thesis, Middle East Technical University, 2010.

[27] C. Baktır, "Simulation-based comparison of some GMTI techniques," Master's thesis, Middle East Technical University, 2009.

[28] M. Eyili, "Multi-target particle filter based track before detect algorithms for spawning targets," Master's thesis, Middle East Technical University, 2014.

[29] M. Sabuncu, "Particle filter based track before detect algorithm for tracking of dim moving targets," Master's thesis, Middle East Technical University, 2012.

[30] G. Sahin and M. Demirekler, "A multidimensional Hough transform algorithm based on unscented transform as a track before detect method," in *IEEE 17th International Conference on Information Fusion*, pp. 1–8, 2014.

[31] M. A. Richards, *Fundamentals of radar signal processing*. McGraw-Hill Education, 2005.

[32] C. V. J. Jakowatz, D. E. Wahl, P. H. Eichel, D. C. Ghiglia, and P. A. Thompson, *Spotlight-Mode Synthetic Aperture Radar: A Signal Processing Approach: A Signal Processing Approach*. Springer Science & Business Media, 2012.

[33] S. R. J. Axelsson, "Position correction of moving targets in SAR imagery," *SAR Image Analysis, Modeling, and Techniques VI*, vol. 5236, no. 3, p. 80, 2004.

[34] H. Hellsten, *Meter-Wave Synthetic Aperture Radar for Concealed Object Detection*. Artech House, 2017.

[35] R. D. Chapman, C. M. Hawes, and M. E. Nord, "Target motion ambiguities in single-aperture synthetic aperture radar," *IEEE Transactions on Aerospace and Electronic Systems*, vol. 46, no. 1, pp. 459–468, 2010.

[36] S. V. Baumgartner and G. Krieger, *Multi-Channel SAR for Ground Moving Target Indication*. 2014.

[37] R. K. Raney, "Synthetic Aperture Imaging Radar and Moving Targets," *IEEE Transactions on Aerospace and Electronic Systems*, vol. AES-7, no. 3, pp. 499–505, 1971.

[38] R. Boulic, N. M. Thalmann, and D. Thalmann, "A Global Human Walking Model With Real-Time Kinematic Personification," no. Girard 1989, pp. 344–358, 1990.

[39] M. Hadzagic, H. Michalska, and E. Lefebvre, "Track-before detect methods in tracking low-observable targets: A survey," *Sensors Trans Mag*, vol. 54, no. 1, pp. 374–380, 2005.

[40] O. Hellwich and H. Mayer, "Extracting line features from synthetic aperture radar (SAR) scenes using a Markov random field model," in *Proceedings of 3rd IEEE International Conference on Image Processing*, vol. 3, pp. 883–886, IEEE, 1996.

[41] R. G. Gallager, *Stochastic processes: theory for applications*. Cambridge University Press, 2013.

[42] J. Arnold, S. W. Shaw, and H. Pasternack, "Efficient target tracking using dynamic programming," *IEEE Transactions on Aerospace and Electronic Systems*, vol. 29, no. 1, pp. 44–56, 1993.

[43] H. Askar, Z. Fu, and Z. Li, "Detecting dim moving point targets using transformation of pixel statistics," in *IEEE 2002 International conference on Communications, Circuits and Systems and West Sino Expositions*, vol. 2, pp. 972–976, IEEE, 2002.

[44] C. Oliver and S. Quegan, *Understanding synthetic aperture radar images*. SciTech Publishing, 2004.

[45] A. C. Frery, H.-J. Muller, C. d. C. F. Yanasse, and S. J. S. Sant'Anna, "A model for extremely heterogeneous clutter," *IEEE transactions on geoscience and remote sensing*, vol. 35, no. 3, pp. 648–659, 1997.

[46] M. Soumekh, *Synthetic aperture radar signal processing*, vol. 7. New York: Wiley, 1999.

[47] "Sarper[TM] online," 2018. `http://www.aselsan.com.tr/en-us/capabilities/radar-systems`.